Hygroscopic growth and CCN activity of secondary organic aerosol produced from dark ozonolysis of gamma-terpinene

Hichem Bouzidi, Layal Fayad, Cécile Coeur, Nicolas Houzel, Denis Petitprez, Alessandro Faccinetto, Junteng Wu, Alexandre Tomas, Jakub Ondráček, Jaroslav Schwarz, et al.

Hygroscopic growth and CCN activity of secondary organic aerosol produced from dark ozonolysis of γ-terpinene

Hichem Bouzidi[1,2,4*‡], Layal Fayad[1‡], Cecile Coeur[1], Nicolas Houzel[1], Denis Petitprez[3], Alessandro Faccinetto[3], Junteng Wu[3‡], Alexandre Tomas[4], Jakub Ondráček[2], Jaroslav Schwarz[2], Vladimír Ždímal[2] and Andreas Zuend[5]

[1] Laboratoire de Physico-Chimie de l'Atmosphère, Université du Littoral Côte d'Opale, Dunkerque, 59140, France.

[2] Institute of Chemical Process Fundamentals of the CAS, Department of Aerosols Chemistry and Physics, Prague, CZ-16502, Czech Republic.

[3] Univ. Lille, CNRS PC2A, 59000 Lille, France.

[4] IMT Lille Douai, Institut Mines-Télécom, Univ. Lille, Centre for Energy and Environment, 59000, Lille, France.

[5] Department of Atmospheric and Oceanic Sciences, McGill University, Montreal, Quebec, H3A 0B9, Canada.

[*]Corresponding author: Hichem Bouzidi (hichem.bouzidi@univ-littoral.fr)

‡These authors contributed equally.

Abstract

The hygroscopic growth factor (*GF*) and cloud condensation nuclei (CCN) activity of secondary organic aerosol (SOA) particles produced during dark ozonolysis of γ-terpinene under different reaction conditions were investigated. The SOA particles were produced in the presence or absence of cyclohexane, an OH scavenger; 1,3,5-trimethylbenzene, an anthropogenic volatile organic compound; and $(NH_4)_2SO_4$ seed particles. A hygroscopicity tandem differential mobility analyzer was used to determine the *GFs* of the SOA particles at RHs ≤ 93%. For some experiments, a CCN counter was used for size-resolved measurement of CCN activation at supersaturation (*S*) in the range of 0.1 to 1%. The single hygroscopicity parameter κ was derived from both the *GF* and CCN measurements. Under subsaturated conditions, all the SOA (except those in the presence of the $(NH_4)_2SO_4$ seeds) showed small *GF* values. These *GF*s demonstrated that SOA mass loading affected the *GF*. A decrease in the SOA mass loading led to increased *GF* and corresponding κ_{GF} values. However, in a supersaturation regime, the SOA mass loading and the size of the particles did not significantly alter the CCN activity of the SOA. Our CCN measurements showed higher κ_{CCN} values (κ_{CCN} = 0.20–0.24) than those observed in most monoterpene ozonolysis studies (κ_{CCN} = 0.1–0.14). This difference may have been due to the presence of the two endocyclic double bonds in the γ-terpinene structure, which may have affected the SOA chemical composition, in contrast to monoterpenes that contain an exocyclic double bond. Our comparisons of sub- and supersaturated conditions showed a larger range of κ values than other experiments. Average κ_{CCN}/κ_{GF} ratios of ~7 and 14 were obtained in the unseeded SOA experiments at low and high SOA mass

loadings, respectively. The average κ_{CCN} of 0.23 indicated that the SOA produced during ozonolysis of γ-terpinene exhibited fairly high CCN activity.

Keywords: Monoterpenes, γ-terpinene, SOA, Hygroscopic growth, CCN activation, Cloud droplet

Graphical abstract

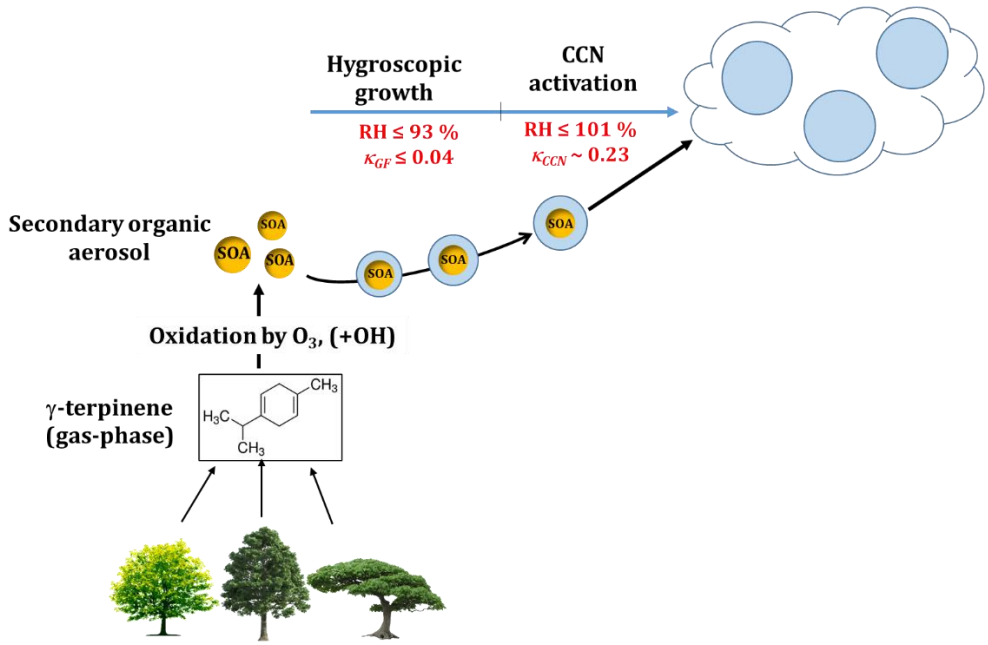

1. Introduction

It has been established that atmospheric aerosols affect the Earth's radiation budget by altering the scattering and absorption of sunlight (direct effect), but also the cloud microphysics and thus ultimately affecting the cloud lifetime and coverage (indirect effect) (Liu and Wang, 2010; IPCC, 2013; Scott et al., 2014; Swietlicki et al., 2017). The magnitude of both effects depends on the hygroscopic properties of atmospheric particles under sub- and supersaturated conditions (Zieger et al., 2010; Väisänen et al., 2016). The hygroscopicity and cloud condensation nuclei (CCN) activity of aerosol particles represents the ability of the particles to interact with water vapor in the surrounding air, which is governed by several chemical-physical properties of the particles, such as their chemical composition, size, physical state and morphology (Mikhailov et al., 2009; Krieger et al., 2012; Swietlicki et al., 2017; Altaf et al., 2018). Large hygroscopic particles can be easily activated as cloud droplets due to the key effect of nucleus size in cloud droplet formation. Whereas, small particles are less efficiently activated into cloud droplets and are more sensitive to the aerosol composition and environmental peak supersaturation during cloud formation (Zhao et al., 2015; Chang et al., 2017).

Atmospheric aerosols are complex mixtures of organic and inorganic components. Secondary organic aerosol (SOA) particles account for a significant mass fraction of tropospheric aerosols (Zhang et al., 2007; Hallquist et al., 2009). SOA particles are produced mainly during gas-phase oxidation of volatile precursors, which originate from a wide variety of biogenic and anthropogenic sources. Some of the oxidation products have a vapor pressure low enough to nucleate or adsorb onto pre-existing particles (Donahue et al., 2014). In addition, it has been shown that interactions between anthropogenic and biogenic volatile organic compounds (VOCs)

can significantly affect the properties of the SOA (Hoyle et al., 2011; Setyan et al., 2014; Moise et al., 2015; Ahlberg et al., 2017).

To describe the ability of dry particles to act as CCN, Petters and Kreidenweis (2007) extended the Köhler theory (Eq. 2; Section 3) by introducing the semi-empirical single hygroscopicity parameter *kappa* (κ) to characterize the water activity of a multicomponent mixture. In theory, κ describes the intrinsic ability to promote water uptake and depends only on the chemical composition of the nuclei (Petters and Kreidenweis, 2013). In practice, κ combines different factors, including solubility and surface tension, that represent CCN activation as a function of the dry particle diameter (Petters et al., 2009b). The simplest form of the parameter κ is based on the assumption of perfect dissolution and no change in the gas-particle partitioning of particle components upon changes in RH (i.e., non-volatile solutes) (Rastak et al., 2017). A key aspect of this parameter is that changes in the apparent κ values may be related to changes in the chemical composition due to chemical reactions (Petters and Kreidenweis, 2013). Therefore, κ is widely used to describe and relate sub- and super-saturated measurements of hygroscopicity and can be incorporated into models used to predict CCN concentrations (Topping et al., 2011). For aerosols of complex or unknown chemical composition, κ can be derived by measuring the particle activity against the water vapor supersaturation at fixed particle size, or equivalently against the particle size at fixed water vapor supersaturation (often denoted κ_{CCN}) (Prenni et al., 2007; Su et al., 2010; Cerully et al., 2011; Petters and Kreidenweis, 2013; Wu et al., 2020). Alternatively, κ can be estimated from the hygroscopic growth factor (*GF*) of the particles under subsaturated conditions with a hygroscopicity tandem differential

mobility analyzer (HTDMA) (often denoted κ_{GF}) (Petters and Kreidenweis, 2013; Cai et al., 2018).

Monoterpenes ($C_{10}H_{16}$), such as α-pinene, β-pinene, limonene and α- and γ-terpinene, represent a large fraction of BVOCs emitted in the atmosphere and are considered to be key contributors to a large fraction of a biogenic SOA (Kanakidou et al., 2005; Tsigaridis et al., 2014; Hodzic et al., 2016; Xu et al., 2018; Yáñez-Serrano et al., 2018; Zhang et al., 2018). The chemistry of monoterpenes in the atmosphere is known to affect CCN activity (Pöschl et al., 2010; Jokinen et al., 2015), as well as radiative forcing, through aerosol-cloud interactions (Kazil et al., 2010; Carslaw et al., 2013; IPCC, 2013).

Previous studies have focused mainly on the hygroscopic growth and CCN activity of SOA particles that are derived from the oxidation of the three main monoterpenes, α-pinene, β-pinene, and limonene, by using a variety of oxidants and reaction conditions (Huff Hartz et al., 2005; VanReken et al., 2005; Varutbangkul et al., 2006; King et al., 2007; Prenni et al., 2007; Duplissy et al., 2008; Engelhart et al., 2008; Asa-Awuku et al., 2009; Jurányi et al., 2009; King et al., 2009; Petters et al., 2009c; Wex et al., 2009; Frosch et al., 2011; Alfarra et al., 2013; Zhao et al., 2016). Most of these studies have suggested that SOA particles that are generated from different precursors can be efficient sources of CCN when the particles are sufficiently large (Petters et al., 2009c). Virkkula et al. (1999) investigated the hygroscopic properties of SOA particles produced during the oxidation of limonene, α-pinene, and β-pinene in the presence and absence of $(NH_4)_2SO_4$ seed particles. The SOA particles that were formed during photooxidation and dark ozonolysis of 100 ppbv of α-pinene and limonene were slightly hygroscopic under subsaturated conditions, with κ_{GF} ranging between 0.04 and 0.06. VanReken et al. (2005) reported CCN activity data suggesting

a dependence on the specific monoterpene SOA precursor (α-pinene, β-pinene or 3-carene), in contrast to studies by Prenni et al. (2007) and Engelhart et al. (2008), who reported comparable CCN activity for these precursors at initial concentrations lower than 40 ppbv. Dependence of the particle composition and/or hygroscopic properties on the initial precursor concentration has been reported in ozonolysis and photooxidation experiments with α-pinene-derived-SOA particles (Duplissy et al., 2008; King et al., 2009; Shilling et al., 2009; Tritscher et al., 2011; Zhao et al., 2015). These studies reported that SOA particles at low mass loading contain more oxygenated materials than those at high mass loading. Zhao et al. (2015) observed size-dependent κ_{CCN} and chemical composition of SOA particles derived from the oxidation of α-pinene and limonene and anthropogenic aromatic precursors and their mixtures in the size range of 50–200 nm. They found that small particles had a higher κ_{CCN} and a higher degree of oxidation, although all the particles were formed from the same reaction mixture, in agreement with previous studies (Tritscher et al., 2011; Frosch et al., 2013). Furthermore, several laboratory studies (Wex et al., 2009; Good et al., 2010b; Massoli et al., 2010; Dusek et al., 2011; Alfarra et al., 2013; Hansen et al., 2015; Pajunoja et al., 2015; Hodas et al., 2016) and field measurements (Cerully et al., 2011; Wu et al., 2013; Bougiatioti et al., 2016) conducted on SOA or mixed organic–inorganic particles (Hodas et al., 2016) have indicated that κ_{GF} and κ_{CCN} can vary substantially and that the κ_{CCN} was usually higher than the κ_{GF}. On the other hand, in some studies, closure between κ_{CCN} and κ_{GF} was achieved within experimental uncertainty under certain conditions (Duplissy et al., 2008; Jurányi et al., 2009; Good et al., 2010b; Dusek et al., 2011). Hence, several studies have discussed the observed discrepancy in behavior (Prenni et al., 2007; Petters et al., 2009c; Wex et al., 2009; Good et al., 2010a; Good et al., 2010b; Poulain et al., 2010; Rastak et al., 2017). The

discrepancies have been attributed to a combination of several effects, including the gradual dissolution of sparingly soluble compounds at high RH, highly non-ideal solution behavior, measurement uncertainties related to HTDMA operation and the surface tension effect (Petters and Kreidenweis, 2013). However, although Rastak et al. (2017) offered plausible explanations that were supported by thermodynamic computations, including the effects of limited organic water solubility and liquid–liquid phase separation and transitions at high RH, the causes have not yet been fully resolved experimentally.

While γ-terpinene is considered one of the most dominant monoterpenes and is measured in significant quantities in biogenic sources (Geron et al., 2000; Esquivel-Hernández et al., 2011; Iqbal et al., 2014), little is known about its SOA ozonolysis formation and properties. γ-terpinene is a monocyclic monoterpene with two substituted endocyclic C=C double bonds, which make it more reactive toward ozone, with a rate constant of 2.1×10^{-16} cm^3 $molecule^{-1}$ s^{-1} (Fayad et al., 2020). γ-terpinene has been commonly detected in emissions from several tree species (Geron et al., 2000) and essential oils (Geron et al., 2000; Iqbal et al., 2014). Nineteen percent of γ-terpinene emissions have been shown to come from *Sequoia sempervirens* and 11% have come from *Umbellularia californica* (Geron et al., 2000). Biogenic hydrocarbon measurements in a tropical forest in Costa Rica indicated significant emissions of γ-terpinene up to 1.5 ppbv in October, which is higher than that of d-limonene (1.3 ppbv), 3-carene (1.1 ppbv) or β-pinene (0.4 ppbv) (Esquivel-Hernández et al., 2011). To date, only a few studies have examined the ozonolysis of γ-terpinene (Lee et al., 2006; Fayad et al., 2020; Xu et al., 2020), indicating that γ-terpinene may be an important contributor to biogenic SOA (Xu et al., 2020; Fayad et al., 2021a). The mechanisms of oxidation of γ-terpinene by O_3 lead to several gas-phase unsaturated first-generation

multifunctional products (Lee et al., 2006; Fayad et al., 2020; Xu et al., 2020) that can further react with ozone to form highly oxidized products, which may affect the SOA yields and properties (especially the O:C values) compared to monoterpenes containing only one double bond, such as α-pinene. Compared to that in limonene, which also contains two double bonds (one endocyclic and one exocyclic), the second endocyclic double bond in γ-terpinene may cause the dissociation of the carbon skeleton (Xu et al., 2020). Therefore, compared to limonene ozonolysis, a greater number of smaller molecular compounds may be produced during γ-terpinene ozonolysis, which may affect the SOA particle properties, including their hygroscopic properties (Xu et al., 2020). Despite significant emissions of γ-terpinene and its high reactivity toward ozone, to the best of our knowledge, the hygroscopic properties and the CCN activity of SOA particles produced during γ-terpinene ozonolysis have not been studied in the literature. We know only one study in which the hygroscopic growth of SOA particles produced from the photooxidation of γ-terpinene in the presence of $(NH_4)_2SO_4$ seed particles under subsaturated conditions (RH ≤ 85%) was investigated (Varutbangkul et al., 2006), and it was reported that the generated SOA particles were slightly hygroscopic based on the growth factors measured at 85% RH.

Given the apparent inconsistency between the hygroscopic properties of different monoterpene oxidation under sub- and supersaturated conditions reported in the literature, we believe that there is a need to study the hygroscopicity of SOA particles produced during γ-terpinene ozonolysis. In this study, we investigated the hygroscopicity of SOA particles produced during dark ozonolysis of γ-terpinene under sub- and supersaturated regimes. The experiments were conducted under different experimental conditions in the atmospheric simulation chamber CHARME (Chamber

for the Atmospheric Reactivity and the Metrology of the Environment) of the LPCA laboratory. The objectives of the present work are to:

i) determine the hygroscopic particle diameter growth and derive the related *GF* and apparent κ_{GF} parameter of the SOA particles formed from γ-terpinene ozonolysis in the absence and presence of anthropogenic VOC 1,3,5-trimethylbenzene (TMB), the OH scavenger cyclohexane (CHEX), and $(NH_4)_2SO_4$ seed particles. Specifically, we report the time series of the aerosol growth factors of each experiment.

ii) measure the CCN activation properties and derive the κ_{CCN} value for a subset of the studied aerosols.

The obtained hygroscopic water uptake under sub- and super-saturated conditions expressed as the κ_{GF} and κ_{CCN} values were compared with the results reported in previous monoterpene ozonolysis studies. The closure between the κ determined at sub- and super-saturated conditions was investigated. To the best of our knowledge, the present study is the first to report the water uptake of SOA particles formed from γ-terpinene ozonolysis under sub- and super-saturated regimes.

2. Experimental setup, instrumentation and protocol

2.1. Chamber description, experimental conditions and methodology

The experiments were carried out in the 9.2 m^3 electropolished stainless steel chamber CHARME (Fig. S1). Details about CHARME have been provided in previous studies (Fayad, 2019; Fayad et al., 2020; Meng et al., 2020). All chamber experiments were carried out at a RH < 2% and room temperature T = 296 ± 2 K. SOA particles were formed via gas-phase dark ozonolysis of γ-terpinene (97%, Sigma–Aldrich) (1) in

the presence or absence of CHEX (98%, Sigma–Aldrich) as an OH scavenger; (2) TMB (98%, Sigma–Aldrich) as an anthropogenic SOA precursor; and (3) $(NH_4)_2SO_4$ seed particles (≥ 99%, Sigma–Aldrich) as inorganic component present in atmospheric particles. An overview of the conditions in all experiments is given in Table 1. In a typical experiment, a known amount of organic compound (γ-terpinene, CHEX and TMB) was directly injected with purified air as the carrier gas into the chamber under a primary vacuum (residual pressure < 5 mbar). Then, the chamber was filled with purified air (Parker Zander KA-MT 1-8 generator) until the pressure exceeded the atmospheric pressure by 10–15 mbar to avoid ambient contamination. The mixture was allowed to equilibrate for 30 min, resulting in a stable precursor concentration, as determined by proton transfer reaction–time-of-flight–mass spectrometry (PTR–ToF–MS Ionicon 1000, Analytic GmbH, Austria). First, two types of experiments were carried out, where the initial concentration of γ-terpinene was varied between low (8–16 ppbv) and high (150–402 ppbv) concentrations (see Table 1). To study the influence of anthropogenic VOCs on SOA hygroscopicity, 5 experiments with γ-terpinene and TMB (Exp #13–16, Table 1) were carried out at a constant molar ratio (1:3) of γ-terpinene: TMB to accommodate a rate constant ratio, $k_{OH+\gamma\text{-terpinene}}/k_{OH+TMB}$, of ~3. In some experiments, the OH radicals produced during the ozonolysis reaction were scavenged by CHEX (Exp #17–20). The amount of injected cyclohexane was enabled 99% of the produced OH radicals to react with CHEX. In three experiments (Exp #20–23), $(NH_4)_2SO_4$ seed particles were used to induce the condensation of low-volatile reaction products onto the particles. Dry seed particles were injected into the chamber using a constant output atomizer (TSI, Model 3076) from an aqueous solution of $(NH_4)_2SO_4$ (0.015 M, during 4 min with an air flow rate of 2.2 L min^{-1}), followed by a silica gel diffusion dryer. The particle number concentration in the chamber was ~ 1.5×10^4 cm^{-}

^{3} with an initial dry size-distribution mode diameter of ~ 55–60 nm (σ_{geo} = 1.6–1.7). The coagulation rates of aerosol particles are generally low at these concentration levels (Hussein et al., 2009; Rim et al., 2012; Yu et al., 2013). No new particle formations were observed (see Figure S3b; Table 1), and the measured particle diameters were larger than those of the initial seed particles, indicating that they existed in an internal mixed state. In all seeded SOA experiments, the condensation process rate becomes equal to the wall loss after 100–120 min. The general approach with polydisperse seed particles leads to mixed sizes of seed species and gives greater uncertainty in determining SOA coating thickness with respect to seed particles (Meyer et al., 2009a). Ozone was added to initialize the oxidation of γ-terpinene in an excess ozone regime using a UV lamp ozone generator (Air Tree Ozone Technology, Model C-L010-DTI). Purified air or pure oxygen gas (>99%) was used depending on the required ozone concentration. The ozone concentration, RH, and temperature were continuously monitored in the chamber throughout the experiments by an ozone monitor (UV photometric, Thermo Scientific 49i) and VAISALA HUMICAP HMT330 sensors. The pressure inside the chamber was controlled by MK Baratron capacitance gauges. The particle mobility size distribution over the size range of 14.6–661.2 nm was characterized with a scanning mobility particle sizer (SMPS, DMA Model 3081, CPC Model 3775, TSI, USA). The SMPS was operated at a fixed sample flow rate of 0.3 L min^{-1}. The sheath:sample flow ratio was fixed at 10:1. For seeded SOA particles, the organic volume fraction (ε_{Org}), defined as the relative organic volume with respect to the total particle volume, was estimated. Using the volume concentration of ammonium sulfate seed particles and the total particle volume measured after ~1 hour, ε_{Org} values of 0.34 and 0.67 were estimated for the seeding experiments at 16 ppbv and 26 ppbv of the initial concentration of γ-terpinene, respectively.

2.2. Particle hygroscopic growth measurements (HTDMA)

A hygroscopic tandem differential mobility analyzer (HTDMA; custom-made at Institute of Chemical Process Fundamentals of the Czech of Academy of Sciences) (Fig. S2) was used to measure online the hygroscopic properties of produced particles. The HTDMA setup and measurement principles have been described in detail elsewhere (Bouzidi et al., 2020; Asadzadeh et al., 2021). Briefly, the polydisperse particles in the chamber were quickly dried to < 5% RH using a silica gel diffusion dryer coupled to a Nafion gas dryer (Perma Pure Inc., USA). The dry polydisperse particles were charged with a RX-soft neutralizer and transformed into quasi monodisperse particles by the 1st DMA (DMA 1). Due to the temporal evolution of the size-distribution of the γ-terpinene-SOA particles, the dry selected diameter obtained by DMA 1 ($D_{(0,\ dry)}$ = 50–180 ± 1 nm) gradually increased over time according to the evolution of the size distribution. The size-selected dry particles, $D_{(0,\ dry)}$, were then exposed to a given RH (20 – ~93%) with a residence time of ~11 s in the humidification section of the HTDMA, which consisted of a Nafion membrane tube (Perma Pure Inc., USA). The particle number size distribution (40–350 nm) of the resulting wet particles was measured by the second DMA (DMA 2) operated with a CPC (TSI Model 3022A, USA), which was used as the particle detection system. HTDMA data were saved only when the difference in the absolute values between the RH of the aerosol flow (RH_4) and sheath flow (RH_3) was ≤ 2% (see Fig. S1). The particle's hygroscopicity, expressed by the mobility diameter hygroscopic growth factor (*GF*) at a given RH (20–93%), was compared to the particle dry size $D_{(0,\ dry)}$ as follows:

$$GF = \frac{D(\mathrm{RH},\ \mathrm{DMA\ 2})}{D_{(0,\ Dry)}(\mathrm{RH} < 2\%, \mathrm{DMA\ 1})} \times \chi \qquad (1)$$

where D(RH, DMA 2) and $D_{(0,\ dry)}$ (RH < 2%, DMA 1) are the mobility diameters of the particle at a given RH (measured by DMA 2) and under the dry conditions of RH < 2% (measured by DMA 1), respectively. χ is the shape correction factor used to convert the mobility diameter (D) into a volume equivalent diameter (d_{ve}) (Gysel et al., 2002). For near-spherical particles, D is equal to d_{ve} (χ = 1). At high RH, particles are usually spherical and compact; hence, d_{ve} and D(RH, DMA 2) are equal, and no shape correction is needed (Gysel et al., 2004). However, dry particles may have irregular shapes; therefore, the measured $D_{(0,\ dry)}$ must be shape-corrected to obtain d_{ve} (Gysel et al., 2002). These irregularities in the dry particles can cause a discrepancy between the measured mobility diameters, $D_{(0,\ dry)}$ and d_{ve}, and may bias the measured *GFs* (Boreddy et al., 2014). Theoretically, the growth factors have to be adjusted by correction factors to account for an overestimation of the experimental dry diameter (Gysel et al., 2004). For example, a correction factor of 1.08 has been determined for cubic dry NaCl particles with a mobility diameter of 100 nm (Gysel et al., 2002).

The raw data were inverted using the *TDMAinv* algorithm developed by (Gysel et al., 2009). Hereafter, the measured *GFs* refer to the mean of the growth factor-probability density function (*GF-PDF*). During the ozonolysis of γ-terpinene, the RH of the humidification section and the second DMA was set to a constant RH in the range of 87-93% for measuring the *GF* at 90% RH. For some experiments (Exps #1, 7, 13, 14, 15, 16, 20, 21, 22, and 23), as the particle nucleation stopped and the mass of the particles reached the maximum value, the RH of the humidification section varied from 93% to ~20%, and the *GFs* were then plotted against the water activity a_w (bulk equilibrium RH) to obtain a humidogram (*GFs* vs. a_w). Assuming that the particles were in equilibrium with their humidified environment, *S* = RH/100 was converted to a_w by removing the Kelvin effect according to Eq. 6, Section 3 (Dawson et al., 2016).

335 The performance of the HTDMA was validated and regularly checked via the
336 atomization of an aqueous $(NH_4)_2SO_4$ solution (0.5 g L^{-1}) and then by drying the
337 droplets using silica-gel diffusion dryers. A deliquescence relative humidity point (DRH)
338 of 80 ± 1% RH and an average *GF* of 1.49 were measured for the ammonium sulfate
339 particles (100 nm), in good agreement with the thermodynamic model AIOMFAC
340 (Zuend et al., 2008). *GF* uncertainties in our experiments were mainly caused by RH
341 and were estimated to be less than 3.5%, 2.5% and < 1.5% for 93%, 90% and < 80%
342 RH, respectively.

343

344 **2.3. CCN measurements**

345 A continuous flow CCN counter (CCNc, DMT-100 Droplet Measurement
346 Technologies, USA) was used to characterize the CCN activity of the produced SOA
347 by measuring the size-resolved CCN activity of monodisperse aerosol particles. In this
348 case, the CCN activity measurements were performed by coupling a differential
349 mobility analyzer (DMA, 3081, TSI, USA) with the CCNc and CPC (Model 3775, TSI
350 USA) (Roberts and Nenes, 2005; Rose et al., 2008; Moore et al., 2010). This method
351 had been successfully used in several previous studies (Asa-Awuku et al., 2008;
352 Duplissy et al., 2008; Engelhart et al., 2008; Moore et al., 2010; Zhao et al., 2015; Zhao
353 et al., 2016). The polydisperse particles were neutralized by a soft X-Ray source
354 neutralizer (TSI, 3077) and then transformed into monodisperse SOA particles with a
355 size range of 60–120 nm by the DMA (operated at a fixed 0.8 L min^{-1} aerosol flow rate
356 with a sheath-to-aerosol flow rate of 10). The classified aerosols were split between
357 the CCNc and the CPC, and then, the concentrations of the cloud condensation nuclei
358 (from the CCNc; CCN) and of the seeding aerosol particles (from the CPC; CN) were
359 simultaneously measured. The flow rate of the CCNc was 0.5 L min^{-1} with a sheath-to-

sample flow rate of 10. The residence time in the CCNc column was approximately 18 s. The supersaturation (*SS* (%)) was calibrated by using dry $(NH_4)_2SO_4$ particles. The activated fraction *AF* ratio (CCN/CN) was plotted versus the *SS* (%) in the range of 0.1–1% to determine the CCN activation curve. Previous studies have shown that the behavior of *AF-SS* spectra strongly depends on the aerosol size distribution (Abdul-Razzak and Ghan, 2000; Snider et al., 2006) and the κ distribution (Cerully et al., 2011; Su et al. 2010). For example, the *AF-SS* curves of the 80 nm SOA particles in Exp. 10 (Figure S5b) showed the typically observed distribution produced by double charged particles. To estimate the hygroscopicity κ of the studied aerosol particles, the experimental CCN spectra are fitted with a modified κ-Köhler model (Eq. 8; Section 3), taking into account both the size distribution and the κ distribution.

3. Data analysis

The saturation ratio, *S*, over an aqueous solution droplet can be described by the Köhler theory (Petters and Kreidenweis, 2007):

$$S = \frac{RH}{100\%} = a_w \exp\left(\frac{4M_w\sigma_{s/a}}{RT\rho_w D_p}\right) \quad (2)$$

where a_w is the mole fraction-based water activity; $\sigma_{s/a}$ is the surface tension of the solution/air interface, which is often assumed to be equal to that of water (0.072 J m^{-2}); ρ_w and M_w are the density and molar mass of water, respectively; D_p is the wet particle diameter relative to the growth factor, i.e., $D_p = D_{dry} \times GF$, where D_{dry} is the dry particle diameter and *R* and *T* are the universal gas constant and absolute temperature, respectively. As detailed in the introduction, Petters and Kreidenweis (2007) proposed a single-parameter expression for hygroscopicity and CCN activity defined through its effect on the water activity of the solution:

$$\frac{1}{a_w} = 1 + \kappa \frac{V_s}{V_w}. \quad (3)$$

where V_s and V_w are the volumes of dry particulate matter and water, respectively.

Assuming volume additivity, and combining Eq. (2) with Eq. (3), an equation defining the "κ-Köhler theory" is written as (Petters and Kreidenweis, 2007):

$$S = \frac{D_p^3 - D_{dry}^3}{D_p^3 - D_{dry}^3(1-\kappa)} \exp\left(\frac{4M_w\sigma_{s/a}}{RT\rho_w D_p}\right). \quad (4)$$

This equation can be used to predict the water uptake in the subsaturated (S < 1) regime, as well as the conditions for cloud droplet activation. κ ~ 1.4 is the upper limit for many hygroscopic species typically found in atmospheric aerosols (e.g., NaCl), whereas κ ~ 0 is expected for non-hygroscopic particles (Petters and Kreidenweis, 2007). κ can be estimated from the pairs of *GF* and RH values provided by the HTDMA under the subsaturated condition (κ_{GF}) by rearranging Eq. (4) as follows:

$$\kappa_{GF} = \frac{(GF^3 - 1)(1 - a_w)}{a_w} \quad (5)$$

when a_w is computed from RH via the following:

$$a_w = RH / \exp\left(\frac{4M_w\sigma_{s/a}}{RT\rho_w D_p}\right) \quad (6)$$

The κ parameter that is determined from *GF* values at a a_w of 85% or 90% can be used to estimate the CCN activity of the particles (Petters and Kreidenweis, 2007). For continuous water uptake systems measured by a HTDMA, according to Dick et al. (2000) and Kreidenweis et al. (2005), HTDMA *GF* values can be parameterized in terms of water activity using a three-parameter curve fit defined as:

$$GF = \left[1 + (a + b \cdot a_w + c \cdot a_w^2)\frac{1 - a_w}{a_w}\right]^{1/3} \quad (7)$$

where *a*, *b* and *c* are three adjustable coefficients that are determined by fitting the measured *GF* data obtained at different RH levels to an expression in a_w. The coefficient values for the experiments that exhibited continuous water uptake are given in Table S1.

To estimate κ from activated fraction-supersaturation (*AF-SS*) CCN measurements, both the studied aerosol size distribution and the distribution of κ were fitted to the CCN spectra, which could be described by a modified κ-Köhler model (Wu et al., 2020):

$$F_a(SS) = \sum_{\kappa=0}^{\infty} \left\{ \frac{1}{2} - \frac{1}{2} erf \left[\frac{ln\, d_p(\kappa, SS) - ln\, \mu_{p,mode} - ln^2\, \sigma_{p,geo}}{\sqrt{2}\, ln\, \sigma_{p,geo}} \right] \right\} p(\kappa) \Delta\kappa \qquad (8)$$

where $\mu_{p,mode}$ and $\sigma_{p,geo}$ are the mode and the geometrical standard deviation of the aerosol size distribution, respectively. *p(*κ*)* is the probability density function of κ, which is also described with a lognormal distribution (Wu et al., 2020):

$$p(\kappa) = \frac{1}{\kappa\, ln\, \sigma_{\kappa,geo} \sqrt{2\pi}} e^{-\frac{\left[ln\, \kappa - ln\, \mu_{\kappa,mode} - ln^2\, \sigma_{\kappa,geo}\right]^2}{2\, ln^2\, \sigma_{\kappa,geo}}} \qquad (9)$$

- where $\mu_{\kappa,mode}$ and $\sigma_{\kappa,geo}$ are the mode and the geometrical standard deviation of κ, respectively. $\mu_{\kappa,mode}$ and $\sigma_{\kappa,geo}$ are the output parameters when the CCN spectra are fitted by the modified model. The uncertainty in κ_{CCN} is derived from *p(*κ*)* curve fitting and its mean value of the half wave (MVHW) and is approximately 20% of the globally measured values.

For $(NH_4)_2SO_4$ (AS) SOA seed particles, the overall value of κ_{CCN} for the aerosols of a given mobility diameter (d_m) was estimated by using the following simple equation, in which the volume-weighted fractions of all participating species were used (Petters and Kreidenweis, 2007):

$$\kappa_{CCN} = \varepsilon_{AS}\kappa_{AS} + \varepsilon_{Org}\kappa_{Org} \quad (10)$$

where ε_{AS} and ε_{Org} are the volume fractions of the $(NH_4)_2SO_4$ and organic species, respectively. Here, κ_{AS} and κ_{Org} are the single parameters of κ for the ammonium sulfate and organic species, respectively.

4. Results and discussion

4.1 Hygroscopic growth factor measurements at subsaturated conditions

This section presents the results of a series of laboratory experiments performed to investigate the hygroscopic growth factors of SOA particles produced during the dark ozonolysis of γ-terpinene in the presence or absence of 1,3,5-trimethylbenzene, cyclohexane, or $(NH_4)_2SO_4$ seed particles. Figure 1 shows the time series of the measured *GFs* at a bulk equilibrium RH of 90% (equivalent to water activity a_w after Kelvin effect correction using the surface tension of pure water (~0.072 J m^{-2} at 298 K)) for SOA produced from (a) ozonolysis of γ-terpinene (Exp #1–12, Table 1), (b) ozonolysis of γ-terpinene in the presence of TMB (Exp #13–16, Table 1) and (c) ozonolysis of γ-terpinene in the presence of CHEX (Exp #17–20, Table 1). The ozonolysis reaction was initiated at t = 0. For experiments at low (8 and 16 ppbv) and high (≥ 150 ppbv) initial precursor mixing ratios, the *GFs* were measured at 18 min and < 2 min after the start of the reactions, respectively.

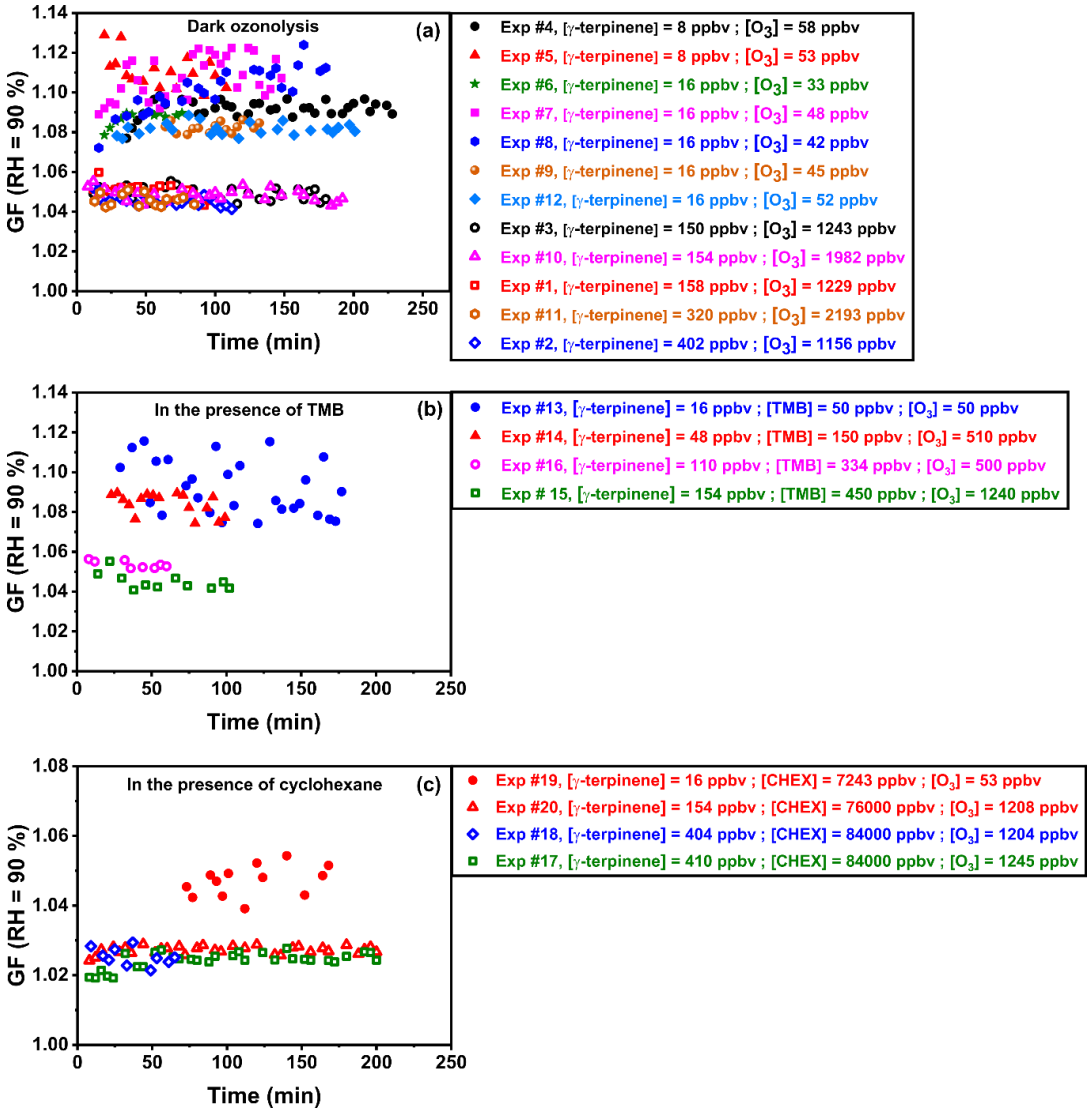

Figure 1. Temporal evolution of the hygroscopic *GFs* at bulk RH (a_w) = 90% and *T* = 296 ± 0.2 for SOA produced from dark ozonolysis of γ-terpinene measured (a) at low (8, 16 ppbv) and high (150 – ~400 ppbv) initial concentrations, (b) low (16, 48 ppbv) and high (110, 154 ppbv) initial precursor concentrations in the presence of TMB, and (c) low (16 ppbv) and high (154 – ~400 ppbv) initial precursor concentrations in the presence of CHEX. The initial mixing ratios of ozone, TMB, and CHEX of each experiment are shown in the legend. Solid and open symbols represent the measured *GFs* (RH = 90%) for SOA produced from the low and high initial concentrations of γ-terpinene. The data are based on 50–180 nm classified dry diameters (see Table 1).

For all experiments, the hygroscopicity of SOA produced during the dark ozonolysis of γ-terpinene (Exp #1–12; Figure 1a) in the presence of TMB (Exp #13–16; Figure 1b) and CHEX (Exp #17–20; Figure 1c) at low and high initial γ-terpinene concentrations and different initial concentrations of ozone showed a narrow range of *GFs*. The results shown in Figure 1 illustrate that the *GF* values were slightly dependent on the initial concentrations of the precursors and ozone. *GFs* of ~1.050–1.120 (Figure 1a) and ~1.053–1.110 (Figure 1b) at a a_w value of 90%, which corresponded to a κ_{GF} of ~0.014–0.040 and κ_{GF} of ~0.015–0.041, respectively, were measured for the SOA produced during dark ozonolysis of γ-terpinene and in the presence of TMB, respectively. The experiments in the presence of CHEX as an OH scavenger (Exp #17–20; Figure 1c) showed the lowest water uptake at an a_w of 90% with measured *GFs* of ~1.024–1.048, corresponding to a κ_{GF} of ~0.008–0.016. These findings were consistent with the findings of Wex et al. (2009) and Yuan et al. (2017), in which the addition of butanol as an OH scavenger decreased the hygroscopicity of the SOA generated from the ozonolysis of monoterpenes. The addition of an OH-radical scavenger has been shown to affect the $[HO_2]/[RO_2]$ ratio and the fate of RO_2 radicals, which could influence the SOA chemical composition and properties (Wex et al., 2009; Henry and Donahue, 2011; Ahmad et al., 2017). As shown in Figure 1, the water uptake of the studied particles under the varying reaction conditions did not show an apparent temporal variation in the *GFs* of all dry sizes, as previously reported (Saathoff et al., 2003; Baltensperger et al., 2005; Varutbangkul et al., 2006). This finding is consistent with that of other monoterpene ozonolysis studies (Prenni et al., 2007; Denjean et al., 2015). Therefore, an average *GF* was calculated for each experiment, and the results are summarized in Table 1. Note that to analyze the potential dependence of the measured *GFs* on particle size, in some experiments, two

or three dry diameters were selected for the HTDMA measurements. However, no significant difference was observed, suggesting that the measured *GF* at a a_w value of 90% and the derived κ_{GF} were relatively insensitive to the selected particle size.

The measured *GFs* of the unseeded SOA (*GFs* ~1.05–1.12) were consistent with the previously obtained measurements of α-pinene + O_3 SOA, which were 1.07 ± 0.01 at 84% RH (Virkkula et al., 1999), 1.07 ± 0.02 at 85% RH (Prenni et al., 2007), 1.04 at 90% RH (Denjean et al., 2015), and a *GF* < 1.05 at a RH of < 98% (Wex et al., 2009). The measured κ_{GF} values (κ_{GF} ~0.014–0.040) were in line with the reported values of κ (0.026) at a RH of 99.2–99.9% for α-pinene SOA obtained in seed-free experiments (Ruehl et al., 2012). Note that our measurements were slightly lower than the unique measurements reported in the literature for the OH-initiated photooxidation of γ-terpinene in the presence of $(NH_4)_2SO_4$, which had a reported *GF* of 1.05 at 85% RH (Varutbangkul et al., 2006). This difference was likely due to the different experimental conditions used in the two studies, which may have affected the chemical composition of the resulting SOA.

As shown in Table 1, the average *GFs* indicated that the initial concentration of the precursors and the oxidation conditions affected the hygroscopic properties of the SOA produced in this study. To better characterize the effects of the initial concentrations on the observed water uptake of the SOA, the average of the measured *GFs* was related to the initial O_3 concentration, and the [TMB]/[γ-terpinene], [CHEX]/[γ-terpinene] and [CHEX]/[O_3] ratios, as illustrated in Figures 2-4. Figures 2a and 2b show the average of the measured *GFs* and the SOA mass loading, respectively, versus those of the initial concentration of O_3 (Exp #1–12). The measured *GFs* clearly appeared to be mass loading-dependent. All the SOA particles produced from low

485 initial γ-terpinene and O_3 concentrations (i.e., low SOA mass loading) showed higher
486 water uptake compared to those in the experiments with higher initial precursor
487 concentrations (higher SOA mass loading). For example, at the lowest mass loading
488 (0.27 μg m^{-3}; Exp #5, Table 1), we measured the greatest *GF* of 1.110 ± 0.020, which
489 corresponded to a κ_{GF} of 0.040 ± 0.004. A similar observation has been reported for
490 several chamber studies (Duplissy et al., 2008; Shilling et al., 2009; Tritscher et al.,
491 2011). Shilling et al. (2009) showed that the aerosol composition of SOA produced
492 from the ozonolysis of α-pinene and the corresponding physical properties were
493 dependent on the total organic mass loading. They indicated that the molecules
494 partitioning into the particle phase at lower mass loadings were more oxygenated than
495 those partitioning at higher loadings, as might be expected on the basis of the
496 structure-activity relationship of vapor pressure for organic molecules (Pankow and
497 Asher, 2008). Duplissy et al. (2008) and Massoli et al. (2010) found that the increase
498 in the water uptake of the SOA produced from the photooxidation of α-pinene at low
499 SOA mass loading was caused by an increase in the oxygen content of components
500 in the particles (i.e., enhanced atomic O:C ratio). Tritscher et al. (2011) found that
501 higher volatility and lower hygroscopicity were generally observed in experiments with
502 high SOA particle masses, consistent with the expected behavior of gas–particle
503 partitioning as a function of precursor loading (Donahue et al., 2009; Zuend and
504 Seinfeld, 2012).

505

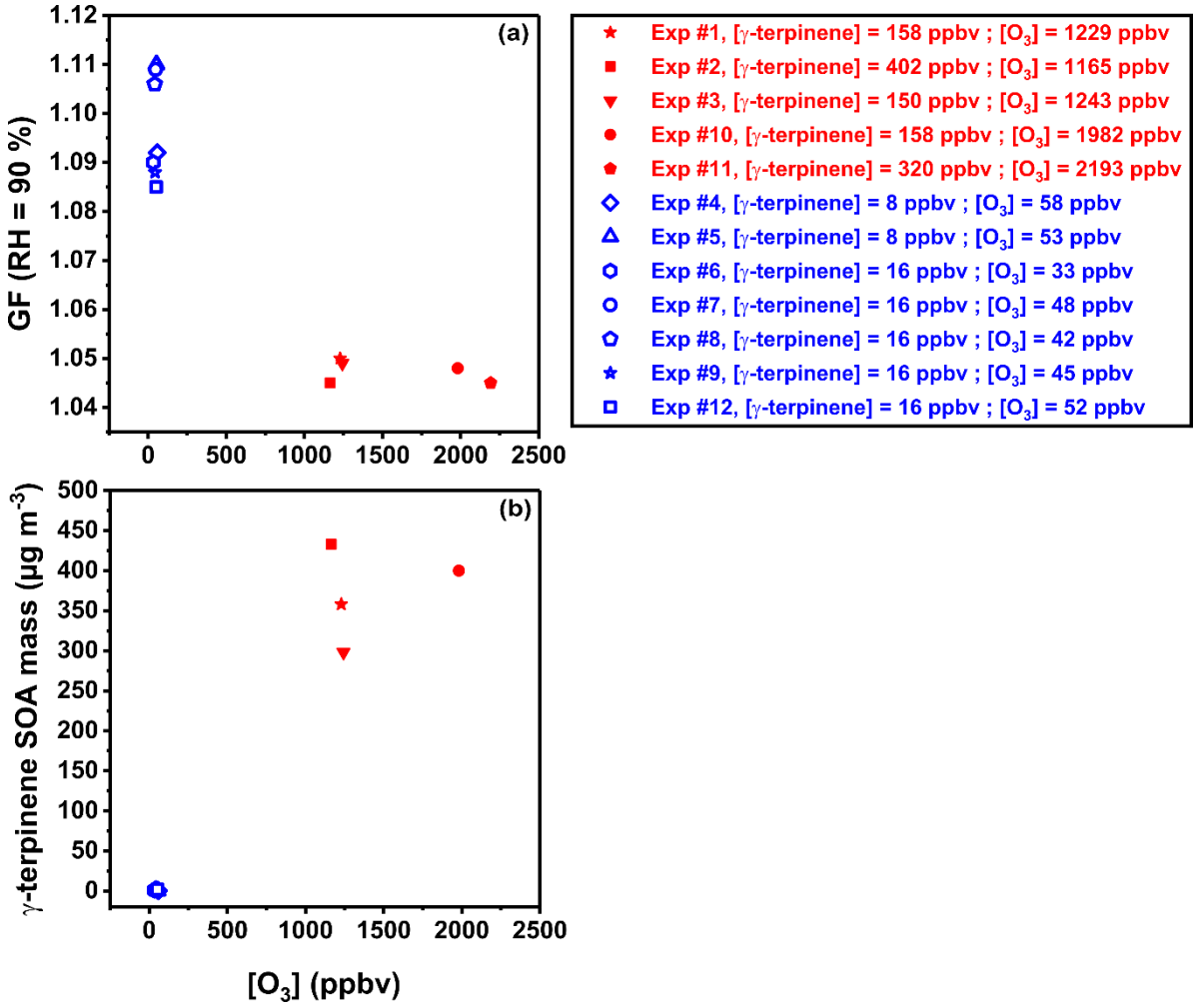

Figure 2: Dependence of the hygroscopic growth factor on the SOA mass loading for SOA produced during the dark ozonolysis of γ-terpinene (Exp #1–12). (a) The hygroscopic *GFs* at bulk RH (a_w) = 90% versus the initial concentration of ozone, (b) γ-terpinene SOA mass loading versus the initial concentration of ozone. The SOA mass loading shown in (b) was measured on the basis of SMPS volume measurements with ρ_{SOA} = 1.

506

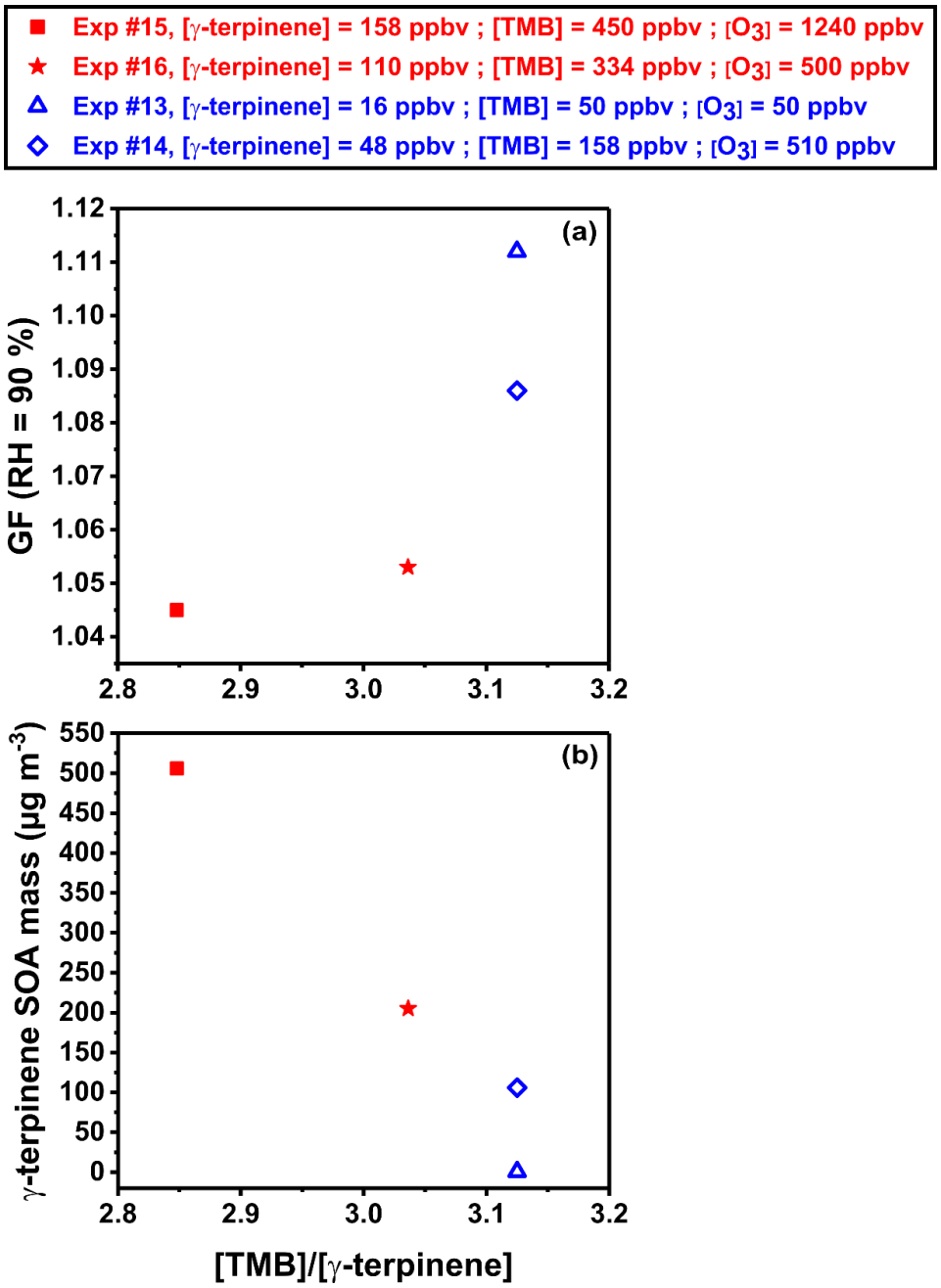

Figure 3: Dependence of the hygroscopic growth factor on the SOA mass loading for SOA produced during the dark ozonolysis of γ-terpinene in the presence of TMB (Exp #13–16). (a) The hygroscopic *GFs* at bulk RH (a_w) = 90% versus the [TMB]/[γ-terpinene] ratio and (b) mixed γ-terpinene-TMB SOA mass loading versus [TMB]/[γ-terpinene] ratio. The SOA mass loading shown in (b) was measured on the basis of the SMPS volume measurements with ρ_{SOA} = 1.

Figure 3 shows the strong dependencies of *GF* and SOA mass loading on the [TMB]/[γ-terpinene] ratio. A decrease in the SOA mass loading (Figure 3b) led to an increase in the γ-terpinene-SOA water uptake (Figure 3a). For comparison, the highest mass loading obtained in Exp #15 (506 μg m^{-3}) from the ozonolysis of 158 ppbv of γ-terpinene in the presence of 450 and 1240 ppbv of TMB and ozone, respectively, showed the lowest *GF* (1.045 ± 0.015). The results from two experiments, #16 and #14, in which the same ozone level (~500 ppbv) was used but the initial concentrations of γ-terpinene and TMB differed, clearly illustrated the effect of the initial concentrations of the precursors on the water uptake of the generated SOA. As shown in Figure 3, a decrease in [γ-terpinene] from 110 to 48 ppbv increased the *GF* from 1.053 ± 0.012 to 1.086 ± 0.017. In addition, the comparison between Exp #13 and Exp #14 showed that the decrease in the initial concentration of γ-terpinene or ozone led to enhanced SOA water uptake. The obtained results showed that the decrease in both initial precursor concentrations and ozone led to a decrease in the SOA mass concentrations and a significant increase in the water uptake. This outcome was attributed to volatile and less-oxygenated vapor condensing at high mass concentrations, thus lowering the measured *GFs* (Tritscher et al., 2011).

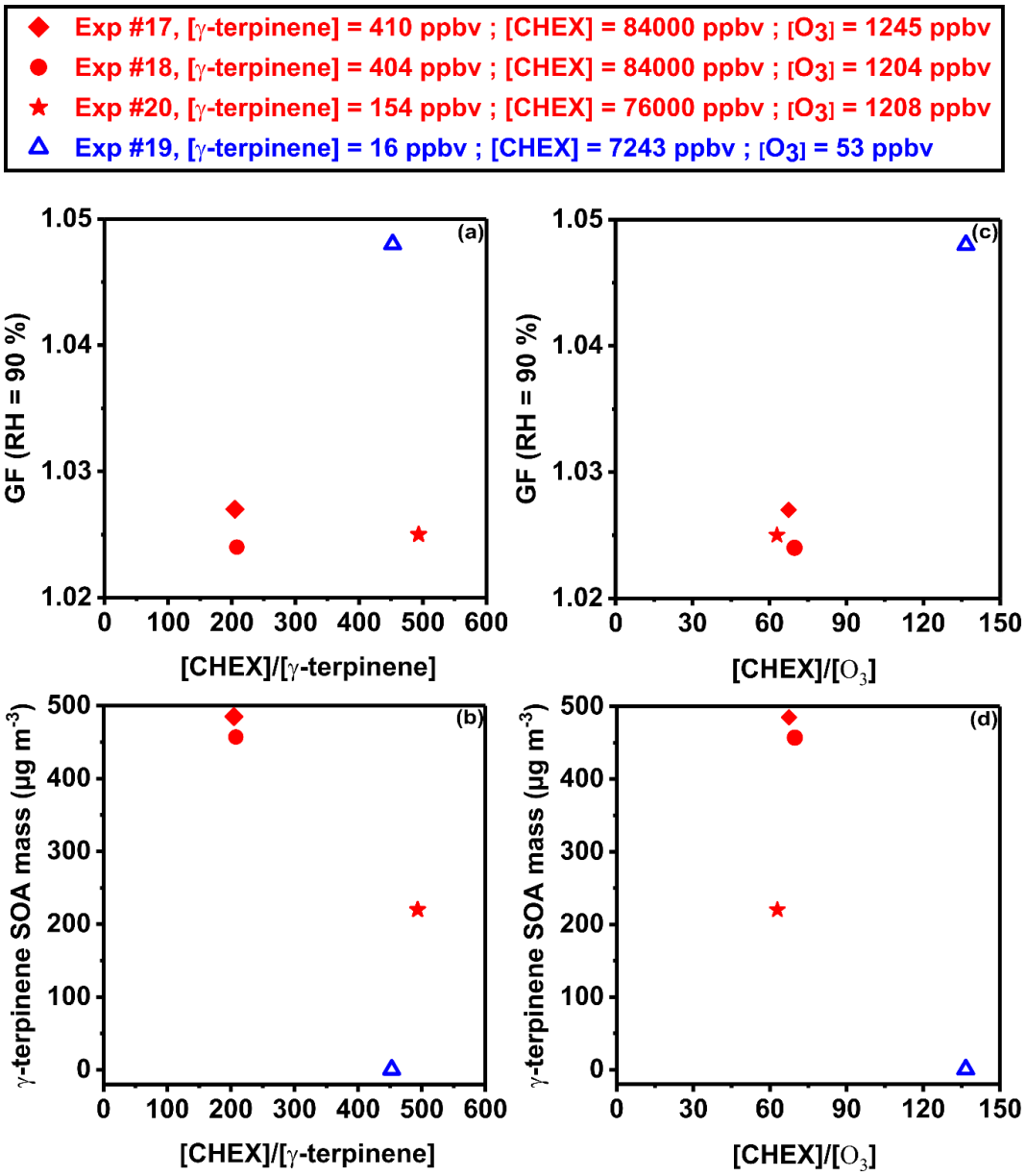

Figure 4: Dependence of the hygroscopic growth factor on the SOA mass loading for SOA produced during the dark ozonolysis of γ-terpinene in the presence of cyclohexane (CHEX) (Exp #17–20). (a) and (c) The hygroscopic *GFs* at bulk RH (a_w) = 90% versus the [CHEX]/[γ-terpinene] and [CHEX]/[O_3] ratios, respectively; (b) and (d) γ-terpinene SOA mass loading versus the [CHEX]/[γ-terpinene] and [CHEX]/[O_3] ratios, respectively. The SOA mass loadings shown in (b) and (d) were measured on the basis of the SMPS volume measurements with ρ_{SOA} = 1.

525

Figure 4 illustrates the water uptake and the SOA mass concentrations for the SOA produced in the presence of cyclohexane. The *GFs* were split into two groups of low and high mass loading relative to the [CHEX]/[γ-terpinene] and [CHEX]/[O_3] ratios. The highest *GF* value (Exp #19; Figures 4a, 4c) was correlated to the lowest SOA mass loading (Fig. 4b, 4d). An increase in *GF* was observed when the initial concentration of γ-terpinene was decreased (thus increasing the [CHEX]/[γ-terpinene] ratio; Figure 4a) or when ozone was decreased (thus increasing the [CHEX]/[O_3] ratio; Figure 4c).

Based on the above analysis of Figures 2–4, it appears that the measured *GFs* were dependent on the initial concentrations of the precursors and ozone, which may have affected the O:C ratio of the formed SOA. Factors that influence the SOA O:C ratio include mass loading, oxidant exposure, and peroxy radical fate (Lambe et al., 2015; Xavier et al., 2019; Afreh et al., 2021). The oxidation of γ-terpinene and TMB by ozone and OH radicals produce peroxy radicals (RO_2), which may then undergo two types of reactions: autoxidation to generate highly oxygenated organic molecules (HOMs) with multiple oxygen-containing functional groups and bimolecular RO_2-RO_2 or RO_2-HO_2 radical reactions (Xavier et al., 2019; Schervish and Donahue, 2020; Schervish and Donahue, 2021). RO_2 radicals ultimately terminate into molecular products depending on whether they derive from the first generation RO_2 (without additional -OOH functional), autoxidation, or RO_2 dimerization (Schervish and Donahue, 2020), which affects the O:C ratio of the aerosol particles. It is known that the lifetime of RO_2 formed through the oxidation of VOCs, and thus its fate, is a key determinant of the reaction mechanism and the chemical composition of the SOA (Pagonis et al., 2019). The RO_2 autoxidation pathway, which competes with bimolecular termination reactions, is highly dependent on the conditions of the

experiment, including both the absolute radical concentrations and the radical ratios (Schervish and Donahue, 2021). For example, in an area that exhibits longer RO_2 lifetimes, such as remote areas, autoxidation, which produces HOMs, is expected to be more prevalent than bimolecular reactions (Zhao et al., 2021). At low initial precursor and/or ozone concentrations, the contribution of HOMs formation from the RO_2 autoxidation is expected to be more important, since the lifetime of RO_2 is sufficiently long for autoxidation to compete with bimolecular reactions (Xavier et al., 2019; Schervish and Donahue, 2020). This non-negligible contribution of HOMs (monomers and dimers) to the particle phase would increase the SOA O:C ratio and thus enhance the water uptake of the generated particles. Whereas, the prevalence of the RO_2-RO_2 radical termination of the first-generation RO_2 (less oxidized) will increase with VOC loading (specifically with the rate of VOC oxidation) (Bianchi et al., 2019), leading to higher concentrations of more volatile compounds. Chemical characterization of the SOA produced during dark ozonolysis of γ-terpinene at high and low initial precursor concentrations with a time-of-flight aerosol mass spectrometer (ToF-AMS) is needed for future clarification of these phenomena.

Table 1: Summary of all experimental results and conditions for the SOA experiments

Exp #	[γ-terpinene] (ppb_v)	[O_3] (ppb)	[CHEX] (ppb)	[TMB] (ppb)	Seeds (#/cm^3)	Number Conc. (#/cm^3)	Mass Conc. (µg/m^3)	*GF* (90%) (D_{dry})	κ_{GF}	κ_{CCN}	Comments
Dark ozonolysis											
1	158	1229	-	-	-	1.2 x10^6	358	1.050 (100-140 nm)	0.017		No CCN
2	402	1156	-	-	-	1.0 x10^7	433	1.045 (100-180 nm)	0.015		No CCN
3	150	1243	-	-	-	9.3 x10^5	298	1.049 (100-140 nm)	0.017		No CCN
4	8	58	-	-	-	3.9 x10^3	0.35	1.092 (55-60 nm)	0.033		No CCN
5	8	53	-	-	-	3.7 x10^3	0.27	1.110 (50-60 nm)	0.040		No CCN
6	16	33	-	-	-	7.5 x10^3	0.95	1.090 (60 nm)	0.031		No CCN
7	16	48	-	-	-	1.2 x10^4	2.25	1.109 (50-90 nm)	0.040		No CCN
8	16	42	-	-	-	1.5 x10^4	2.64	1.106 (50-90 nm)	0.039		No CCN
9	16	45	-	-	-	1.5 x10^4	1.96	1.088 (57-82 nm)	0.030		No CCN
10	154	1982	-	-	-	1.1 x10^6	400	1.048 (80-150 nm)	0.016	0.219	d_m = 80 nm
										0.240	d_m = 120 nm
11	320	2193	-	-	-	1.4 x10^6	909	1.045 (80-150 nm)	0.015	-	No CCN
12	16	52	-	-	-	1.5 x10^4	2.01	1.085 (50-80 nm)	0.029	0.198	d_m =60 nm
										0.198	d_m =80 nm
Dark ozonolysis + TMB											
13	16	50	-	50	-	1580	0.8	1.112 (66-100 nm)	0.041	-	No CCN
14	48	510	-	150	-	1.5 x10^5	106	1.086 (80, 150 nm)	0.031	-	No CCN
15	158	1240	-	450	-	5.9 x10^5	506	1.045 (140 nm)	0.015	-	No CCN
16	110	500	-	334	-	1.1 x10^5	205	1.053 (150 nm)	0.018	-	No CCN
Dark ozonolysis + cyclohexane (CHEX)											
17	410	1245	84000	-	-	1.2 x10^7	485	1.027 (150 nm)	0.009	-	No CCN
18	404	1204	84000	-	-	1.1 x10^7	457	1.024 (150 nm)	0.008	-	No CCN
19	16	53	7243	-	-	1.6 x10^3	0.52	1.048 (55-70 nm)	0.016	-	No CCN
20	154	1208	76000	-	-	9.7 x10^5	220	1.025 (100 nm)	0.008	-	No CCN
Dark Ozonolysis + ammonium sulfate seeds											
21	16	52	-	-	1.5 x10^4 [a]	1.5 x10^4 [a]	14.9 [a]	1.700 (60-110 nm) [a]	0.440 [a]	-	DRH~78% [b]
						1.5 x10^4 [b]	-	1.440 (90 nm) [b]	0.220 [b]	0.550 [b]	d_m =90 nm [b]
22	16	47	-	-	1.7 x10^4 [a]	1.7 x10^4 [a]	15.3 [a]	1.690 (60-110 nm) [a]	0.430 [a]	-	No CCN
						1.6 x10^4 [b]	-	1.450 (60, 95 nm) [b]	0.230 [b]	-	DRH ~77% [b]
23	26	54	-	-	1.6 x10^4 [a]	1.6 x10^4 [a]	15.4 [a]	1.720 (60-110 nm) [a]	0.460 [a]	-	No CCN
						1.5 x10^4 [b]	-	1.220 (80, 105 nm) [b]	0.090 [b]	-	DRH ~76% [b]

- *[a] The data are presented for pure ammonium sulfate; [b] The data are presented for SOA particles internally mixed with ammonium sulfate seed particles.*
- *Global uncertainty for κ_{GF} is approximately 10%.*
- *The uncertainty in κ_{CCN} is derived from p(κ) curve fitting and its mean value of the half wave (MVHW) and is globally 20% of the measured values.*

584 Humidograms, which show hygroscopic growth curves versus water activity for
585 SOA produced during the ozonolysis of γ-terpinene in the absence and presence of
586 CHEX and TMB at various particle sizes (Fig. 5; Fig. S4a), indicate that the generated
587 SOAs were slightly hygroscopic and underwent continuous water uptake with
588 increasing RH and no visible deliquescence. These humidograms are consistent with
589 the humidograms of SOA formed by the oxidation of monoterpenes and
590 sesquiterpenes (Varutbangkul et al., 2006).

591

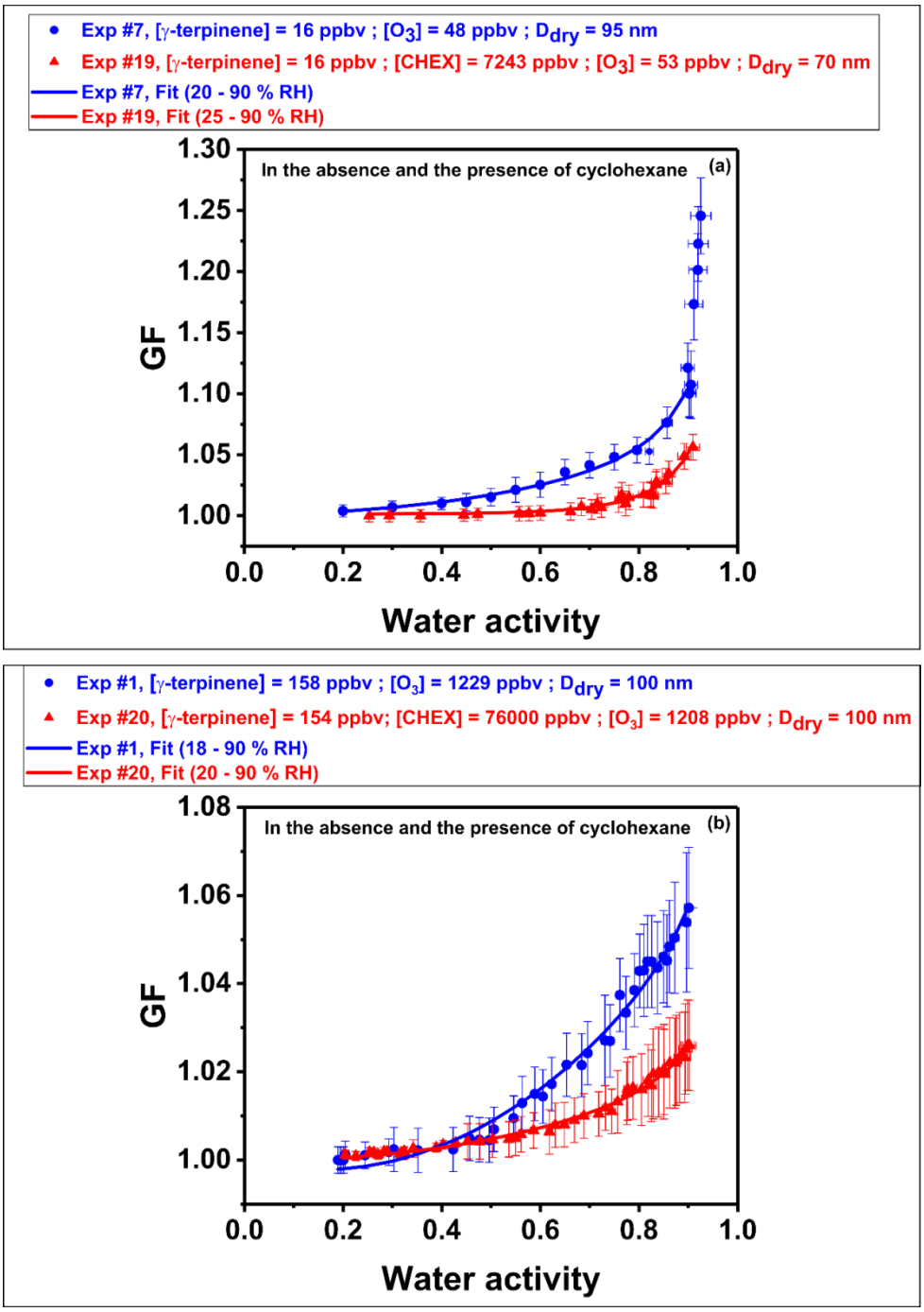

Figure 5: Hygroscopic growth factors for SOA produced from the ozonolysis of γ-terpinene as a function of water activity (a) in the absence and in the presence of cyclohexane at low initial precursor concentrations (16 ppbv; Exp #7 and 19, respectively) and (b) in the absence and in the presence of cyclohexane at high initial precursor concentrations (~158 ppbv; Exp #1 and 20, respectively). The fit of the

measurements to Eq. (7) is shown and the fitted *GF* parameterization data are listed in Table S1.

In the presence of cyclohexane (Fig. 5a, 5b), the hygroscopic growth curves were slightly lower than those in the absence of CHEX for ~a_w > 60%. The hygroscopic behavior in the RH range of 20 – 93% shown in Figure 5a and Figure S4a might indicate the expected change in water uptake for low and moderately hygroscopic organic aerosols, which switch from a water-poor to a water-rich phase at high RH (near 92% RH) (Gorkowski et al., 2019). This behavior may be a result of the gradual dissolution of sparingly soluble organic compounds at increasing RH (Rastak et al., 2017). Figure S4b shows the RH-dependent *GFs* of seed-SOA particles derived from γ-terpinene at the initial concentrations of 16 ppbv (Exp #21) and 26 ppbv (Exp #23). At the beginning of the experiments, *GF* was ~1.720 at 90% RH, which was equal to the measurement of pure $(NH_4)_2SO_4$ (Figure S3a). After the reaction was initiated, *GF* decreased continuously as γ-terpinene was consumed, and the oxidation products were partitioned onto $(NH_4)_2SO_4$ seed particles continuously until the *GF* reached a value of 1.420 for 16 ppbv (Exp #21 and 22; ε_{Org} ~0.34) or 1.220 for 26 ppbv (Exp #23; ε_{Org} ~0.67) of the precursor (see Table 1 and Fig. S3a (SI)). A reasonable hypothesis for this observation is that the organic oxidation products were less hygroscopic than $(NH_4)_2SO_4$. A similar reduction in *GF* in the presence of $(NH_4)_2SO_4$ was observed for the hygroscopicity of SOA produced from different monoterpenes and oxygenated terpenes (Virkkula et al., 1999; Cocker III et al., 2001; Saathoff et al., 2003; Varutbangkul et al., 2006; Wang et al., 2021). No new particle formation was observed during the experiments in which SOA was produced from γ-terpinene in the presence of $(NH_4)_2SO_4$ seed particles (Table 1; Fig. S3b). All experiments showed narrow *GF* distributions for each dry size selected in the HTDMA, suggesting that SOA particles

of the same diameter had similar chemical compositions and hence were internally mixed. The hygroscopic growth curves of the formed SOA particles showed little to no water uptake (*GF* ~1) at low and moderate RH (~73%), but steeply increased particle diameter near full deliquescence at ~ 76% RH (DRH). Slightly more gradual water uptake was observed with increasing organic mass fraction (Exp #23; $[\gamma\text{-terpinene}]_0$ = 26 ppbv; ε_{Org} ~0.67), indicating that a partial amount of $(NH_4)_2SO_4$ may have been dissolved in the mixed organic–inorganic aqueous aerosol solution since organic compounds can affect the solubility of $(NH_4)_2SO_4$ (Choi and Chan, 2002; Marcolli et al., 2004). The DRH of $(NH_4)_2SO_4$ was slightly shifted by the presence of the secondary organic material produced during the ozonolysis of γ-terpinene. This outcome is in agreement with several theoretical and experimental studies reporting that the secondary organic material that is produced from certain biogenic and anthropogenic precursors affects the DRH transition of $(NH_4)_2SO_4$ (Meyer et al., 2009b; Bertram et al., 2011; Smith et al., 2011; Smith et al., 2012; Smith et al., 2013). As expected, both humidograms showed a reduction in the *GFs* measured at 90% RH compared to the pure $(NH_4)_2SO_4$ particles. The *GFs* at 90% a_w were 1.430 (κ_{GF} = 0.250 ± 0.025) and 1.220 (κ_{GF} = 0.100 ± 0.010) for the mixed system generated at 16 and 26 ppbv, respectively. These values are respectively 20% and 44% lower than the measured *GFs* of pure $(NH_4)_2SO_4$ ($\kappa \approx 0.61$; Petters and Kreidenweis (2007)).

4.2 CCN measurements

Figure 6 illustrates the average CCN activation curves in the absence of $(NH_4)_2SO_4$ for two different electrical mobility diameters (d_m) at low SOA mass loading ($[\gamma\text{-terpinene}]_0$ = 16 ppbv; $[O_3]_0$ = 52 ppbv; Exp #12; Table 1)) and at high SOA loading

([γ-terpinene]$_0$ = 154 ppbv; [O_3]$_0$ = 1982 ppbv Exp #10; Table 1). Figure 7 shows the CCN activation curve of the SOA particles that are internally mixed with $(NH_4)_2SO_4$ (Exp #21, [γ-terpinene]$_0$ = 16 ppbv; [O_3]$_0$ = 47 ppbv; ε_{Org} ~0.34). The data represent the average of the data obtained from three full scans.

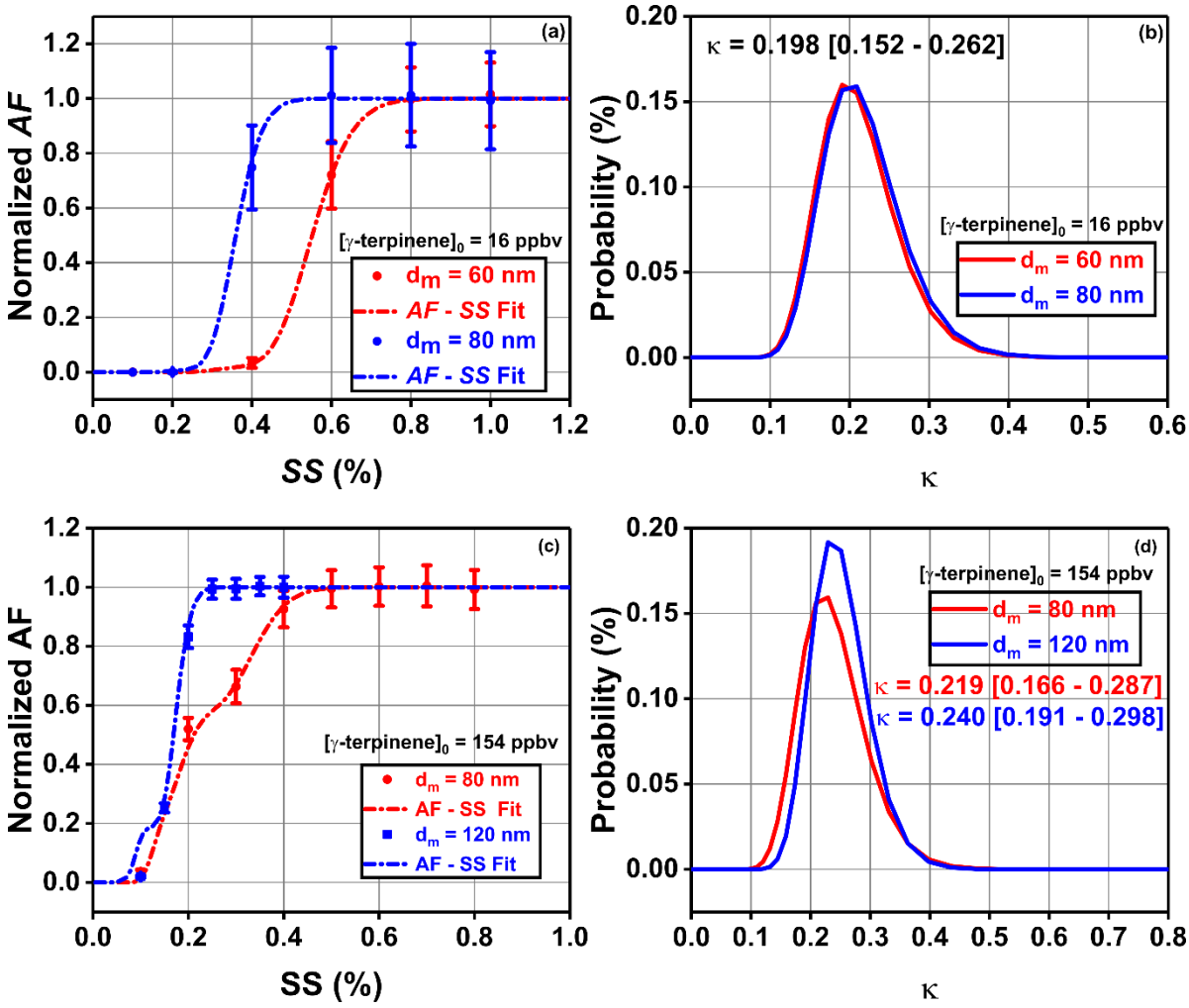

Figure 6: Average CCN activation curves recorded for SOA derived from γ-terpinene ozonolysis at [γ-terpinene]$_0$ = 16 (Exp #12) and 154 ppbv (Exp #10), respectively. (a, c) CCN activation fraction (*AF*) as a function of supersaturation (*SS* (%)). The lines in Figures (a) and (c) are fitted CCN activated fraction curves considering the measured size distributions (Section 3). The error bars in Figures (a) and (c) represent the combined uncertainties calculated from the standard deviations of

repeated CCN and CN measurements. (b, d) The expression of the single-parameter hygroscopicity κ_{CCN} as a probability density function according to Eq. (9).

For CCN measurements at low γ-terpinene concentration (16 ppbv) (low SOA mass loading), d_m values of 60 nm and 80 nm were selected to study the influence of the particle dry size on κ_{CCN}. The particle production and growth represented by the typical "banana plot" showed a single nucleation mode that appeared shortly after the injection of γ-terpinene (see Figure S5a), with a peak number concentration of 1.5×10^4 cm^3. The generated particles did not activate at *SS* of 0.1–0.4% for the first 70 min of the reaction (< 30 CCN cm^{-3}; CN ~ 150 cm^{-3}). Therefore, the CCN measurements were performed at *SS* of 0.1–1% for a d_m of 60 nm and 80 nm. The DMA transfer function (Figure S5b) showed a negligible double-charge fraction compared to the single-charge fraction. The red and blue lines in Figure 6b are the fitted curves for the probability density function $p(\kappa)$ in the form of Eq. (9) at a d_m of 60 and 80 nm, respectively. The identical curves suggest that the κ_{CCN} is independent from the size parameter for the SOA generated from 16 ppbv γ-terpinene and 52 ppbv ozone. The $p(\kappa)$ values shown in Figure 6b were calculated from the fitted size-selected activation fraction (*AF)* – *SS* data (Figure 6a). A κ_{CCN} between 0.152 and 0.262 (average κ_{CCN} = 0.20) can be inferred from these curves. These results were consistent with κ_{CCN} values between 0.14 and 0.23 for α-pinene and mixed monoterpene SOAs, as reported by Engelhart et al. (2008).

Regarding CCN measurements of particles generated from a high SOA mass loading ($[\gamma\text{-terpinene}]_0$ = 154 ppbv, $[O_3]_0$ = 1982 ppbv; Exp #10; Figures 6c, 6d), the nucleation and growth of the produced particles showed a single mode (Figure S6a)

665 with a peak number concentration of 1.1×10^6 that was reached in ~2 min (Table 1). At
666 a d_m of 80 nm, the DMA transfer function (Figure S6b), showed that particles carrying
667 double and even triple charges were not negligible compared to 120 nm particles
668 (Figure S6c). The comparison of the measured average particle probability
669 distributions shown in Figure 6d suggests that κ_{CCN} is independent of the particle size
670 for the produced SOA. Taking into consideration the multimodality of d_m, $p(\kappa)$ spans a
671 range of 0.166-0.287 at 80 nm and 0.191-0.298 at 120 nm, in good agreement with the
672 average κ_{CCN} value of 0.20 (0.152-0.262) determined for γ-terpinene-SOA produced at
673 a low initial concentration of 16 ppbv.

674 From the limited number of CCN measurements, it appears that the initial
675 precursor concentration and the particle size did not significantly alter the CCN activity
676 of the SOA. This finding is in agreement with some studies (Prenni et al., 2007;
677 Duplissy et al., 2008; Engelhart et al., 2008; Jurányi et al., 2009) that indicated the
678 initial precursor concentrations had no influence on the CCN activity of the resulting
679 SOA. This conclusion has to be taken with caution since size-dependent κ_{CCN} values
680 have been observed (Zhao et al., 2015; Prisle et al., 2019). Prisle et al. (2019)
681 observed a size-dependent variation in the CCN activity of pollenkitt from olive, poplar,
682 and ragweed. Zhao et al. (2015) discovered an apparent size-dependent κ_{CCN} (and
683 SOA composition) of SOA particles obtained from the photooxidation of various
684 precursors, such as boreal tree emissions, monoterpenes, and a mixture of α-pinene,
685 limonene, and toluene. The size-dependence of κ_{CCN} might indicate a heterogeneous
686 chemical composition (Winkler et al., 2012; Zhao et al., 2015). For example, Winkler
687 et al. (2012) observed size-dependent composition changes from smaller to larger-
688 sized particles, indicating that the Kelvin effect (and perhaps kinetic/diffusion effects
689 during growth) can play an important role in the growth and composition of biogenic

nanoparticles. Furthermore, Ovadnevaite et al. (2017) demonstrated that κ_{CCN} at critical supersaturation exhibited size dependence not related to a chemical composition change; e.g., for pure aqueous $(NH_4)_2SO_4$ particles, a κ_{CCN} of 0.589 was predicted for 50 nm dry diameter particles, while a κ_{CCN} of 0.633 was predicted for 100 nm dry diameter particles. The γ-terpinene-derived SOA in the present study generally exhibited higher κ_{CCN} (0.20–0.24) than that of previous studies (0.09–0.23) of SOA produced from α-pinene, β-pinene, limonene, 3-carene and their mixtures (Huff Hartz et al., 2005; Prenni et al., 2007; Engelhart et al., 2008; Wex et al., 2009). Prenni et al. (2007) reported a κ_{CCN} value of 0.10 ± 0.04 for SOAs generated by dark ozonolysis of α-pinene, β-pinene, and 3-carene. Wex et al. (2009) reported a κ_{CCN} value of 0.10 ± 0.04 for the SOA derived from dark ozonolysis of α-pinene. Engelhart et al. (2008) found κ_{CCN} values for the SOA produced during dark ozonolysis of α-pinene and mixed monoterpenes ranging between 0.11 and 0.14 using a DMT CCN counter and between 0.14 and 0.23 using a static CCN counter. The latter values were in line with the κ_{CCN} values (0.11–0.14) determined by Huff Hartz et al. (2005) at high *SS* (1%) (obtained using a static CCN counter). However, Engelhart et al. (2008) reported that a larger range in κ_{CCN} was expected when a static CCN counter was used due to the greater uncertainty of the measurements.

The SOA particles produced in this study during the dark ozonolysis of γ-terpinene are relatively good CCN: they are less active than pure $(NH_4)_2SO_4$ ($\kappa_{CCN} \approx 0.61$) but more active than sesquiterpenes ($\kappa_{CCN} < 0.1$) (Huff Hartz et al., 2005; Tang et al., 2012; Frosch et al., 2013). However, our κ_{CCN} values (0.20–0.24; Exp #12 and Exp #10) were also much higher than the κ_{GF} values (0.016–0.029; Exp #12 and Exp #10) measured for the same precursor and under the same oxidation conditions but in

714 the subsaturated water vapor regime. The discrepancy between κ_{CCN} and κ_{GF} is
715 discussed in Section 4.3. Size-resolved CCN measurements are needed for further
716 analysis of the ozonolysis of γ-terpinene with different initial precursor concentrations
717 and electrical mobility diameters to verify whether the initial conditions and the SOA
718 size selection affect the κ_{CCN} values.

719 For SOA particles internally mixed with $(NH_4)_2SO_4$ (Exp #21, $[\gamma\text{-terpinene}]_0$ = 16
720 ppbv; $[O_3]_0$ = 47 ppbv; ε_{Org} ~0.34; Figure 7), the CCN activation spectrum measured at
721 a d_m of 90 nm displayed $p(\kappa)$ values spanning a range of 0.375-0.691 with an average
722 κ_{CCN} of 0.55.

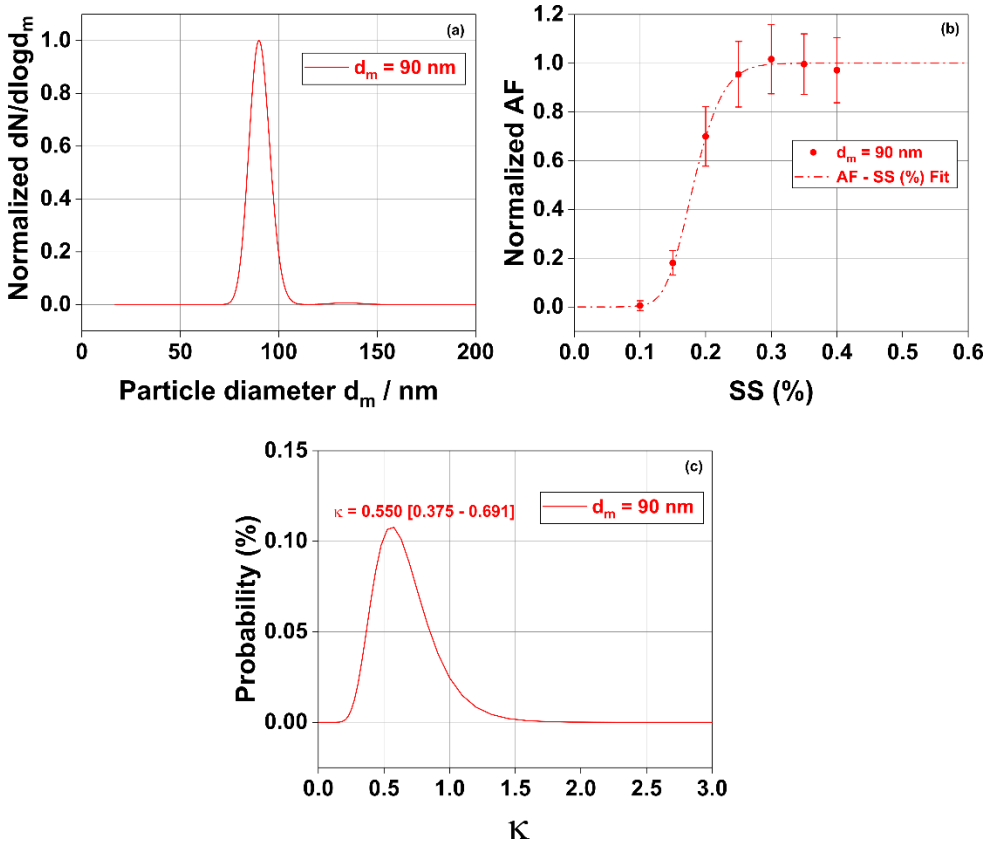

Figure 7. CCN activation curves recorded for SOA particles internally mixed with ammonium sulfate ($[\gamma\text{-terpinene}]_0$ = 16 ppbv, $[O_3]_0$ = 47 ppbv). (a) Normalized d_m

distribution of SOA particles with an electrical mobility diameter d_m of 90 nm. (b) The CCN activation fraction (*AF*) as a function of supersaturation (*SS* (%)). The lines in Figure (b) are fitted CCN activated fraction curves considering the measured size distributions. The error bars in Figure (b) represent the combined uncertainties, which take into account the standard deviations estimated from the repeated CCN and CN measurements under the same conditions. (c) The expression of the single-parameter hygroscopicity κ_{CCN} as a probability density function according to Eq. (9).

723 The SOA particles formed during this experiment exhibited higher CCN activity
724 than pure SOA particles obtained during the ozonolysis of γ-terpinene, which was
725 expected due to the added hygroscopicity effect of the salt fraction. The measured
726 κ_{CCN} was similar to that of pure $(NH_4)_2SO_4$ and indicated that the organic species
727 produced in this seeded experiment (estimated ε_{Org} ~0.34) at a d_m of 90 nm did not
728 substantially affect the CCN activity of the mixed particles. A κ_{CCN} of 0.47, in good
729 agreement with the experimental κ_{CCN}, was calculated by using the simple mixing rule
730 (Eq. 10) with a $\kappa_{CCN,\ (NH4)2SO4}$ of 0.61 and a $\kappa_{CCN,\ Org}$ of 0.20.

731 4.3 Hygroscopicity and CCN activity closure

732 As shown in Table 1 (Exp #10, Exp #12 and Exp #21), the CCN activity obtained
733 from the CCNc measurements was higher than that obtained from the HTDMA
734 measurements. Average κ_{CCN}/κ_{GF} ratios of ~7 and ~14 were determined for SOA
735 particles at low (Exp #12) and high (Exp #10) SOA mass loadings, respectively, and a
736 lower κ_{CCN}/κ_{GF} ratio of ~2.5 (Exp #21) was determined for the internally mixed SOA–
737 $(NH_4)_2SO_4$ particles. A discrepancy between κ values expressed under sub- or
738 supersaturated conditions has been obtained in several previous laboratory and field

739 measurements of organic aerosols but is not yet fully understood (Carrico et al., 2008;
740 Good et al., 2010b; Irwin et al., 2010; Massoli et al., 2010; Cerully et al., 2011; Dusek
741 et al., 2011; Alfarra et al., 2013; Wu et al., 2013; Hansen et al., 2015; Bougiatioti et al.,
742 2016; Dawson et al., 2016). The gap discrepancies between κ_{GF} and κ_{CCN} values
743 suggest a mechanism in the subsaturated regime that leads to reduced water uptake
744 compared to that taken up under the supersaturated condition and depends on the
745 SOA chemical composition (Wittbom et al., 2018). The question is whether this
746 discrepancy is due to the particle properties produced or to the operating principle of
747 the instruments used. Among the possible explanations are:

748 (1) the solubility limitations of the sparingly soluble components of the
749 multicomponent SOA (Petters et al., 2009c; Petters and Kreidenweis, 2013; Wittbom
750 et al., 2018);

751 (2) a non-ideal solution mixing behavior within the particles that cannot be
752 represented by a single hygroscopicity parameter (Petters et al., 2009a; Petters et al.,
753 2009c; Rastak et al., 2017; Liu et al., 2018); the latter including liquid–liquid phase
754 separation at high RH, e.g., in the form of a relatively sharp transition from water-poor
755 to water-rich highly dilute aqueous organic droplets (Rastak et al., 2017; Gorkowski et
756 al., 2019);

757 (3) surface tension effects and related assumptions that affect observed
758 κ values (Wex et al., 2009; Ovadnevaite et al., 2017; Prisle et al., 2019);

759 (4) a combination of the above.

760 While detailed thermodynamic models have provided clear indications for a real
761 gap between κ_{GF} and κ_{CCN} consistent with predictions, to date it is not clear how these
762 effects could be probed individually and reliably in experiments. The problem is further

763 complicated by the occurrence of those effects in correspondence to the sharp
764 changes in water uptake and composition between 98% and 100% RH.

765 The apparent presence of sparingly water-soluble components is supported by
766 the water uptake measurements shown in Figure 5a (Exp #7) and Figure S4a (Exp
767 #16), which might indicate a gradual dissolution of slightly water-soluble components
768 that would cause a switch from a water-poor to a water-rich phase state at high RH.
769 However, while low polarity and hygroscopicity may suggest low water solubility, we
770 emphasize that sparingly soluble organic species do not need to be in a solid-state at
771 lower RH; in contrast, low solubility can be understood as a liquid–liquid miscibility
772 limitation at a given RH, which is closely related to the phenomenon of liquid–liquid
773 phase separation (LLPS). Measurements of *GFs* at higher RHs (> 93%) may provide
774 useful insights into the continuous or discontinuous growth factor behavior that has
775 been observed very close to the point of CCN activation (Wex et al., 2009; Good et al.,
776 2010b; Mikhailov et al., 2021). Rastak et al. (2017) provided measurements and model
777 predictions consistent with non-ideal mixing and LLPS as key effects for observed
778 sharp changes between κ_{GF} and κ_{CCN} at high RH. For example, LLPS was observed
779 at high RH values (> 95%) in particles containing secondary organic material free of
780 inorganic salts derived from the biogenic precursors α-pinene, limonene, and β-
781 caryophyllene (Renbaum-Wolff et al., 2016; Song et al., 2017) and from subpollen
782 particles (Mikhailov et al., 2021). The same effects may play key roles in the apparent
783 hygroscopicity change of the SOA produced from the ozonolysis of γ-terpinene in this
784 study. Furthermore, surface–active compounds in the aerosol particles can cause an
785 increase in the apparent CCN activation efficiency of aerosol particles by reducing the
786 surface tension in the growing droplets, even at high RH, than expected when a surface
787 tension equivalent to that of water was assumed (Facchini et al., 2000; Prisle et al.,

2008; Wex et al., 2008; Wex et al., 2009; Sareen et al., 2013; Ruehl et al., 2016; Zhao et al., 2016; Forestieri et al., 2018; Davies et al., 2019). At low RH (< 95%), the effect of the surface tension on the particle surface–air interface is negligible (Hodas et al., 2016). However, Wex et al. (2009) and Wittbom et al. (2018) found that a reduction in surface tension could only partially explain the discrepancy between κ values determined in both regimes in their experiments. In addition, the co-condensation of semi-volatile organic compounds (due to changes in RH in the instruments) (Topping and McFiggans, 2012) may play an important role and may need to be considered in future analysis of the dynamic CCN activity of SOA.

As described in Section 2.2, the accuracy of the determined *GFs* is sensitive to the (dry) particle shape. Non-spherical shapes can lead to an underestimation of *GFs*. In another study by our group (Fayad et al., 2021b), the use of cryo-transmission electron microscopy combined with energy–dispersive X-Ray spectroscopy (cryo-TSEM-EDX) measurements for γ-terpinene-derived SOA particles showed that the particles at dry conditions (RH of ~2 %) were spherical and in a viscous physical state. Therefore, we conclude that no shape correction factor was needed to correct the HTDMA data for a possible overestimation of the dry volume equivalent diameter in this study (Kreidenweis et al., 2005).

5. Conclusion

This study was focused on the hygroscopic growth and CCN activity of SOA particles derived from the gas-phase reaction of ozone with γ-terpinene at different initial precursor concentrations. The SOA particles were produced in the presence or absence of CHEX, which is an OH scavenger; TMB, which is an anthropogenic VOC; and ammonium sulfate as seed particles. In the absence of seed particles and under

subsaturated conditions, the particles were found to be slightly hygroscopic, with κ_{GF} values of 0.02–0.04 obtained for particles 50–180 nm in diameter. In addition, our study shows that the water uptake of the produced SOA was dependent upon on the reaction conditions. The measured hygroscopic growth factors and their corresponding κ_{GF} values were highly dependent on the SOA mass loading. An increase in the water uptake was observed with a decreasing SOA mass loading.

The hygroscopic growth curves (*GF* vs. a_w) of the SOA formed in the absence or presence of TMB or CHEX exhibited continuous water uptake without a clear deliquescence signal upon hydration. However, the hygroscopic growth curves of the SOA produced in this study in the presence of $(NH_4)_2SO_4$ seeds showed an increase in the diameter of the particles at a deliquescence RH of ~76% of $(NH_4)_2SO_4$ in the mixed particles, which was slightly lower than the deliquescence of pure $(NH_4)_2SO_4$. Under supersaturated conditions, the SOA mass loading and the size of the selected particles did not significantly affect the CCN activity, as indicated by κ_{CCN} values ranging between 0.20 and 0.24 (average κ_{CCN} ~0.23). The κ_{CCN} values found in this study were clearly higher than those measured in previous monoterpene ozonolysis studies (κ_{CCN} from 0.09 to 0.14), in which a DMT CCN counter had been used. The larger κ_{CCN} values found in this study may have been results of the presence of the two endocyclic C=C double bonds in the γ-terpinene structure, which may have affected the chemical composition and the properties of the generated SOA. An average κ_{CCN} value of ~0.23 demonstrated that the dark ozonolysis of γ-terpinene was an efficient source of CCN (for particles of sufficient size) in the atmosphere. Closure analysis of κ_{GF} derived from HTDMA measurements and κ_{CCN} determined from CCN measurements showed significant discrepancy, with κ_{CCN} values that were much

higher than κ_{GF} values, as shown by average ratios κ_{CCN}/κ_{GF} of ~7 and ~17 for low and high SOA mass loading. This ratio was lower for the internally mixed SOA–$(NH_4)_2SO_4$ particles (κ_{CCN}/κ_{GF} ~2.5; ε_{Org} ~0.34) produced in this study. This discrepancy in hygroscopicity can be attributed to the presence of slightly soluble materials, non-ideal mixing behavior within the particles, possible surface tension effects, differing behaviors of the aerosols in the instruments, or a combination of these factors. Data from HTDMA and CCN measurements for the same aerosol systems are insightful, yet they are not sufficient to map out the transition between a water-poor regime with relatively low hygroscopicity under subsaturated conditions and a water-rich regime with substantially higher apparent hygroscopicity under supersaturated conditions. System-specific modeling studies are needed to resolve this gap.

To the best of our knowledge, this study provides the first hygroscopic growth and CCN activity measurements for SOA particles produced through the dark ozonolysis of γ-terpinene. More research is required to improve our understanding of the hygroscopic properties of SOA produced from γ-terpinene photooxidation and reaction with nitrate radicals. Furthermore, our study highlights the need to conduct further studies to investigate the hygroscopic properties of SOA produced from the oxidation of α-phellandrene (another monoterpene containing endocyclic C=C double bonds). This study supports the use of κ ranging between 0.1 and 0.2 as a simplified, yet accurate, single parameter to represent the CCN activation of SOA material in large-scale atmospheric and climate models.

CRediT authorship contribution statement

Hichem Bouzidi: Conceptualization; Methodology; Validation; Investigation; Resources; Writing - Original Draft; Writing – review & editing; Visualization; Supervision; Project administration. **Layal Fayad:** Conceptualization; Methodology; Validation; Investigation; Writing - Original Draft; Writing – review & editing; Visualization. **Cecile Coeur:** Conceptualization; Methodology; Validation; Resources; Writing – review & editing; Visualization; Project administration; Funding acquisition; Supervision. **Nicolas Houzel:** Investigation; Resources. **Denis Petitprez:** Conceptualization; Methodology; Validation; Resources; Writing – review & editing; Visualization; Project administration; Funding acquisition; Supervision. **Alessandro Faccinetto:** Conceptualization; Methodology; Validation; Investigation; Resources; Writing - Original Draft; Writing – review & editing; Visualization; Funding acquisition; Supervision. **Junteng Wu:** Conceptualization; Methodology; Validation; Investigation; Writing - Original Draft; Writing – review & editing; Visualization. **Alexandre Tomas:** Conceptualization; Methodology; Validation; Resources; Writing – review & editing; Visualization; Project administration; Funding acquisition; Supervision. **Ondracek Jakub**: Methodology; Resources; Writing – review & editing. **Jaroslav Schwarz:** Methodology; Resources; Writing – review & editing. **Vladimir Zdimal:** Methodology; Resources; Writing – review & editing; Writing – review & editing; Funding acquisition. **Andreas Zuend:** Conceptualization; Writing - Original Draft; Writing – review & editing.

Acknowledgments

This work was supported by the infrastructure project of the MEYS of the Czech Republic ACTRIS-CZ [grant LM201822]; the Czech Science Foundation [grant

Number 17-19798S]; and the ERDF project “ACTRIS-CZ RI” [grant Number CZ.02.1.01/0.0/0.0/16_013/0001315]. We further acknowledge support by the Natural Sciences and Engineering Research Council of Canada (NSERC) [grant RGPIN/04315–2014]. This work was supported by the CaPPA project (Chemical and Physical Properties of the Atmosphere) funded by the French National Research Agency (ANR-11-LABX-0005-01) and the CLIMIBIO program supported by the Hauts-de-France Regional Council, the French Ministry of Higher Education and Research and the European Regional Development Fund. The PhD grant given to Layal Fayad was funded by ULCO (Université du Littoral - Côte d’Opale) and PMCO (Pôle Métropolitain Côte d’Opale). The IRENE research program is also acknowledged for funding through the “Equipements Phares” call for projects.

References

Afreh, I.K., Aumont, B., Camredon, M., Barsanti, K.C., 2021. Using GECKO-A to derive mechanistic understanding of secondary organic aerosol formation from the ubiquitous but understudied camphene. Atmos. Chem. Phys. 21, 11467-11487.

Ahlberg, E., Falk, J., Eriksson, A., Holst, T., Brune, W.H., Kristensson, A., Roldin, P., Svenningsson, B., 2017. Secondary organic aerosol from VOC mixtures in an oxidation flow reactor. Atmospheric Environment 161, 210-220.

Ahmad, W., Coeur, C., Cuisset, A., Coddeville, P., Tomas, A., 2017. Effects of scavengers of Criegee intermediates and OH radicals on the formation of secondary organic aerosol in the ozonolysis of limonene. Journal of Aerosol Science 110, 70-83.

Alfarra, M.R., Good, N., Wyche, K.P., Hamilton, J.F., Monks, P.S., Lewis, A.C., McFiggans, G., 2013. Water uptake is independent of the inferred composition of secondary aerosols derived from multiple biogenic VOCs. Atmos. Chem. Phys. 13, 11769-11789.

Altaf, M.B., Dutcher, D.D., Raymond, T.M., Freedman, M.A., 2018. Effect of Particle Morphology on Cloud Condensation Nuclei Activity. ACS Earth and Space Chemistry 2, 634-639.

Asa-Awuku, A., Engelhart, G.J., Lee, B.H., Pandis, S.N., Nenes, A., 2009. Relating CCN activity, volatility, and droplet growth kinetics of β-caryophyllene secondary organic aerosol. Atmos. Chem. Phys. 9, 795-812.

Asa-Awuku, A., Sullivan, A.P., Hennigan, C.J., Weber, R.J., Nenes, A., 2008. Investigation of molar volume and surfactant characteristics of water-soluble organic compounds in biomass burning aerosol. Atmos. Chem. Phys. 8, 799-812.

Asadzadeh, B., Bouzidi, H., Bisson, R., Ondráček, J., Schwarz, J., Lahib, A., Ždímal, V., 2021. Hygroscopicity of secondary marine organic aerosols: Mixtures of alkylammonium salts and inorganic components. Science of The Total Environment 790, 148131.

Baltensperger, U., Kalberer, M., Dommen, J., Paulsen, D., Alfarra, M.R., Coe, H., Fisseha, R., Gascho, A., Gysel, M., Nyeki, S., Sax, M., Steinbacher, M., Prevot, A.S.H., Sjögren, S., Weingartner, E., Zenobi, R., 2005. Secondary organic aerosols from anthropogenic and biogenic precursors. Faraday Discussions 130, 265-278.

Bertram, A.K., Martin, S.T., Hanna, S.J., Smith, M.L., Bodsworth, A., Chen, Q., Kuwata, M., Liu, A., You, Y., Zorn, S.R., 2011. Predicting the relative humidities of liquid-liquid phase separation, efflorescence, and deliquescence of mixed particles of ammonium sulfate, organic material, and water using the organic-to-sulfate mass ratio of the particle and the oxygen-to-carbon elemental ratio of the organic component. Atmospheric Chemistry and Physics 11, 10995-11006.

Bianchi, F., Kurtén, T., Riva, M., Mohr, C., Rissanen, M.P., Roldin, P., Berndt, T., Crounse, J.D., Wennberg, P.O., Mentel, T.F., Wildt, J., Junninen, H., Jokinen, T., Kulmala, M., Worsnop, D.R., Thornton, J.A., Donahue, N., Kjaergaard, H.G., Ehn, M., 2019. Highly Oxygenated Organic Molecules (HOM) from Gas-Phase Autoxidation Involving Peroxy Radicals: A Key Contributor to Atmospheric Aerosol. Chemical Reviews 119, 3472-3509.

Boreddy, S.K.R., Kawamura, K., Jung, J., 2014. Hygroscopic properties of particles nebulized from water extracts of aerosols collected at Chichijima Island in the western North Pacific: An outflow region of Asian dust. Journal of Geophysical Research: Atmospheres 119, 167-178.

Bougiatioti, A., Bezantakos, S., Stavroulas, I., Kalivitis, N., Kokkalis, P., Biskos, G., Mihalopoulos, N., Papayannis, A., Nenes, A., 2016. Biomass-burning impact on CCN number, hygroscopicity and cloud formation during summertime in the eastern Mediterranean. Atmos. Chem. Phys. 16, 7389-7409.

Bouzidi, H., Zuend, A., Ondráček, J., Schwarz, J., Ždímal, V., 2020. Hygroscopic behavior of inorganic–organic aerosol systems including ammonium sulfate, dicarboxylic acids, and oligomer. Atmospheric Environment 229, 117481.

Cai, M., Tan, H., Chan, C.K., Qin, Y., Xu, H., Li, F., Schurman, M.I., Liu, L., Zhao, J., 2018. The size-resolved cloud condensation nuclei (CCN) activity and its prediction based on aerosol hygroscopicity and composition in the Pearl Delta River (PRD) region during wintertime 2014. Atmos. Chem. Phys. 18, 16419-16437.

Carrico, C.M., Petters, M.D., Kreidenweis, S.M., Collett Jr., J.L., Engling, G., Malm, W.C., 2008. Aerosol hygroscopicity and cloud droplet activation of extracts of filters from biomass burning experiments. Journal of Geophysical Research: Atmospheres 113.

Carslaw, K.S., Lee, L.A., Reddington, C.L., Pringle, K.J., Rap, A., Forster, P.M., Mann, G.W., Spracklen, D.V., Woodhouse, M.T., Regayre, L.A., Pierce, J.R., 2013. Large contribution of natural aerosols to uncertainty in indirect forcing. Nature 503, 67.

Cerully, K.M., Raatikainen, T., Lance, S., Tkacik, D., Tiitta, P., Petäjä, T., Ehn, M., Kulmala, M., Worsnop, D.R., Laaksonen, A., Smith, J.N., Nenes, A., 2011. Aerosol hygroscopicity and CCN activation kinetics in a boreal forest environment during the 2007 EUCAARI campaign. Atmos. Chem. Phys. 11, 12369-12386.

Chang, D.Y., Lelieveld, J., Tost, H., Steil, B., Pozzer, A., Yoon, J., 2017. Aerosol physicochemical effects on CCN activation simulated with the chemistry-climate model EMAC. Atmospheric Environment 162, 127-140.

Choi, M.Y., Chan, C.K., 2002. The effects of organic species on the hygroscopic behaviors of inorganic aerosols. Environmental Science & Technology 36, 2422-2428.

Cocker III, D.R., Clegg, S.L., Flagan, R.C., Seinfeld, J.H., 2001. The effect of water on gas–particle partitioning of secondary organic aerosol. Part I: α-pinene/ozone system. Atmospheric Environment 35, 6049-6072.

Davies, J.F., Zuend, A., Wilson, K.R., 2019. Technical note: The role of evolving surface tension in the formation of cloud droplets. Atmospheric Chemistry and Physics 19, 2933-2946.

Dawson, K.W., Petters, M.D., Meskhidze, N., Petters, S.S., Kreidenweis, S.M., 2016. Hygroscopic growth and cloud droplet activation of xanthan gum as a proxy for marine hydrogels. Journal of Geophysical Research: Atmospheres 121, 11,803-811,818.

Denjean, C., Formenti, P., Picquet-Varrault, B., Camredon, M., Pangui, E., Zapf, P., Katrib, Y., Giorio, C., Tapparo, A., Temime-Roussel, B., Monod, A., Aumont, B., Doussin, J.F., 2015. Aging of secondary organic aerosol generated from the ozonolysis of α-pinene: effects of ozone, light and temperature. Atmos. Chem. Phys. 15, 883-897.

Dick, W.D., Saxena, P., McMurry, P.H., 2000. Estimation of water uptake by organic compounds in submicron aerosols measured during the Southeastern Aerosol and Visibility Study. Journal of Geophysical Research: Atmospheres 105, 1471-1479.

Donahue, N.M., Robinson, A.L., Pandis, S.N., 2009. Atmospheric organic particulate matter: From smoke to secondary organic aerosol. Atmospheric Environment 43, 94-106.

Donahue, N.M., Robinson, A.L., Trump, E.R., Riipinen, I., Kroll, J.H., 2014. Volatility and Aging of Atmospheric Organic Aerosol, in: McNeill, V.F., Ariya, P.A. (Eds.), Atmospheric and Aerosol Chemistry. Springer Berlin Heidelberg, Berlin, Heidelberg, pp. 97-143.

Duplissy, J., Gysel, M., Alfarra, M.R., Dommen, J., Metzger, A., Prevot, A.S.H., Weingartner, E., Laaksonen, A., Raatikainen, T., Good, N., Turner, S.F., McFiggans, G., Baltensperger, U., 2008. Cloud forming potential of secondary organic aerosol under near atmospheric conditions. Geophysical Research Letters 35, n/a-n/a.

Dusek, U., Frank, G.P., Massling, A., Zeromskiene, K., Iinuma, Y., Schmid, O., Helas, G., Hennig, T., Wiedensohler, A., Andreae, M.O., 2011. Water uptake by biomass burning aerosol at sub- and supersaturated conditions: closure studies and implications for the role of organics. Atmos. Chem. Phys. 11, 9519-9532.

Engelhart, G.J., Asa-Awuku, A., Nenes, A., Pandis, S.N., 2008. CCN activity and droplet growth kinetics of fresh and aged monoterpene secondary organic aerosol. Atmos. Chem. Phys. 8, 3937-3949.

Esquivel-Hernández, G., Madrigal-Carballo, S., Alfaro-Solís, R., Sibaja-Brenes, J.P., Valdés-González, J., 2011. First Measurements of Biogenic Hydrocarbons in Air in a Tropical Cloudy Forest, Monteverde, Costa Rica. Journal of Chemistry and Chemical Engineering 5.

Facchini, M.C., Decesari, S., Mircea, M., Fuzzi, S., Loglio, G., 2000. Surface tension of atmospheric wet aerosol and cloud/fog droplets in relation to their organic carbon content and chemical composition. Atmospheric Environment 34, 4853-4857.

Fayad, L., 2019. Characterization of the new atmospheric simulation chamber CHARME, and study of the ozonolysis reaction of a biogenic VOC, the γ-terpinene

Caractérisation de la nouvelle chambre de simulation atmosphérique CHARME et étude de la réaction d'ozonolyse d'un COV biogénique, le γ-terpinène. Université du Littoral Côte d'Opale.

Fayad, L., Coeur, C., Fagniez, T., Secordel, X., Houzel, N., Mouret, G., 2020. Kinetic and mechanistic study of the gas-phase reaction of ozone with γ-terpinene. Atmospheric Environment, 118073.

Fayad, L., Coeur, C., Houzel, N., Deboudt, K., Sécordel, X., Bouzidi, H., Mouret, G., 2021a. Formation of secondary organic aerosols from the reaction of γ-terpinene with ozone: yields and morphology. Atmospheric Environment 262, 118600.

Fayad, L., Coeur, C., Houzel, N., Deboudt, K., Sécordel, X., Bouzidi, H., Mouret, G., 2021b. Formation of secondary organic aerosols from the reaction of γ-terpinene with ozone: yields and morphology. Atmospheric Environment, 118600.

Forestieri, S.D., Staudt, S.M., Kuborn, T.M., Faber, K., Ruehl, C.R., Bertram, T.H., Cappa, C.D., 2018. Establishing the impact of model surfactants on cloud

condensation nuclei activity of sea spray aerosol mimics. Atmos. Chem. Phys. 18, 10985-11005.

Frosch, M., Bilde, M., DeCarlo, P.F., Jurányi, Z., Tritscher, T., Dommen, J., Donahue, N.M., Gysel, M., Weingartner, E., Baltensperger, U., 2011. Relating cloud condensation nuclei activity and oxidation level of α-pinene secondary organic aerosols. Journal of Geophysical Research: Atmospheres 116, n/a-n/a.

Frosch, M., Bilde, M., Nenes, A., Praplan, A.P., Jurányi, Z., Dommen, J., Gysel, M., Weingartner, E., Baltensperger, U., 2013. CCN activity and volatility of β-caryophyllene secondary organic aerosol. Atmos. Chem. Phys. 13, 2283-2297.

Geron, C., Rasmussen, R., R. Arnts, R., Guenther, A., 2000. A review and synthesis of monoterpene speciation from forests in the United States. Atmospheric Environment 34, 1761-1781.

Good, N., Coe, H., McFiggans, G., 2010a. Instrumentational operation and analytical methodology for the reconciliation of aerosol water uptake under sub- and supersaturated conditions. Atmos. Meas. Tech. 3, 1241-1254.

Good, N., Topping, D.O., Duplissy, J., Gysel, M., Meyer, N.K., Metzger, A., Turner, S.F., Baltensperger, U., Ristovski, Z., Weingartner, E., Coe, H., McFiggans, G., 2010b. Widening the gap between measurement and modelling of secondary organic aerosol properties? Atmos. Chem. Phys. 10, 2577-2593.

Gorkowski, K., Preston, T.C., Zuend, A., 2019. Relative-humidity-dependent organic aerosol thermodynamics via an efficient reduced-complexity model. Atmos. Chem. Phys. 19, 13383-13407.

Gysel, M., McFiggans, G.B., Coe, H., 2009. Inversion of tandem differential mobility analyser (TDMA) measurements. Journal of Aerosol Science 40, 134-151.

Gysel, M., Weingartner, E., Baltensperger, U., 2002. Hygroscopicity of Aerosol Particles at Low Temperatures. 2. Theoretical and Experimental Hygroscopic Properties of Laboratory Generated Aerosols. Environmental Science & Technology 36, 63-68.

Gysel, M., Weingartner, E., Nyeki, S., Paulsen, D., Baltensperger, U., Galambos, I., Kiss, G., 2004. Hygroscopic properties of water-soluble matter and humic-like organics in atmospheric fine aerosol. Atmos. Chem. Phys. 4, 35-50.

Hallquist, M., Wenger, J.C., Baltensperger, U., Rudich, Y., Simpson, D., Claeys, M., Dommen, J., Donahue, N.M., George, C., Goldstein, A.H., Hamilton, J.F., Herrmann, H., Hoffmann, T., Iinuma, Y., Jang, M., Jenkin, M.E., Jimenez, J.L., Kiendler-Scharr, A., Maenhaut, W., McFiggans, G., Mentel, T.F., Monod, A., Prévôt, A.S.H., Seinfeld, J.H., Surratt, J.D., Szmigielski, R., Wildt, J., 2009. The formation, properties and impact of secondary organic aerosol: current and emerging issues. Atmospheric Chemistry and Physics 9, 5155-5236.

Hansen, A.M.K., Hong, J., Raatikainen, T., Kristensen, K., Ylisirniö, A., Virtanen, A., Petäjä, T., Glasius, M., Prisle, N.L., 2015. Hygroscopic properties and cloud condensation nuclei activation of limonene-derived organosulfates and their mixtures with ammonium sulfate. Atmos. Chem. Phys. 15, 14071-14089.

Henry, K.M., Donahue, N.M., 2011. Effect of the OH Radical Scavenger Hydrogen Peroxide on Secondary Organic Aerosol Formation from α-Pinene Ozonolysis. Aerosol Science and Technology 45, 696-700.

Hodas, N., Zuend, A., Schilling, K., Berkemeier, T., Shiraiwa, M., Flagan, R.C., Seinfeld, J.H., 2016. Discontinuities in hygroscopic growth below and above water saturation for laboratory surrogates of oligomers in organic atmospheric aerosols. Atmospheric Chemistry and Physics 16, 12767-12792.

Hodzic, A., Kasibhatla, P.S., Jo, D.S., Cappa, C.D., Jimenez, J.L., Madronich, S., Park, R.J., 2016. Rethinking the global secondary organic aerosol (SOA) budget: stronger production, faster removal, shorter lifetime. Atmos. Chem. Phys. 16, 7917-7941.

Hoyle, C.R., Boy, M., Donahue, N.M., Fry, J.L., Glasius, M., Guenther, A., Hallar, A.G., Huff Hartz, K., Petters, M.D., Petäjä, T., Rosenoern, T., Sullivan, A.P., 2011. A review of the anthropogenic influence on biogenic secondary organic aerosol. Atmos. Chem. Phys. 11, 321-343.

Huff Hartz, K.E., Rosenørn, T., Ferchak, S.R., Raymond, T.M., Bilde, M., Donahue, N.M., Pandis, S.N., 2005. Cloud condensation nuclei activation of monoterpene and sesquiterpene secondary organic aerosol. Journal of Geophysical Research: Atmospheres 110.

Hussein, T., Hruška, A., Dohányosová, P., Džumbová, L., Hemerka, J., Kulmala, M., Smolík, J., 2009. Deposition rates on smooth surfaces and coagulation of aerosol particles inside a test chamber. Atmospheric Environment 43, 905-914.

IPCC, 2013. Climate change 2013: The Physical Science Basis, Contri-bution of Working Group I to the Fifth Assessment of the Inter-governmental Panel on Climate Change.

Iqbal, M.A., Kim, K.-H., Ahn, J.H., 2014. Monoterpenes released from fruit, plant, and vegetable systems. Sensors (Basel, Switzerland) 14, 18286-18301.

Irwin, M., Good, N., Crosier, J., Choularton, T.W., McFiggans, G., 2010. Reconciliation of measurements of hygroscopic growth and critical supersaturation of aerosol particles in central Germany. Atmos. Chem. Phys. 10, 11737-11752.

Jokinen, T., Berndt, T., Makkonen, R., Kerminen, V.-M., Junninen, H., Paasonen, P., Stratmann, F., Herrmann, H., Guenther, A.B., Worsnop, D.R., Kulmala, M., Ehn, M., Sipilä, M., 2015. Production of extremely low volatile organic compounds from biogenic emissions: Measured yields and atmospheric implications. Proceedings of the National Academy of Sciences 112, 7123-7128.

Jurányi, Z., Gysel, M., Duplissy, J., Weingartner, E., Tritscher, T., Dommen, J., Henning, S., Ziese, M., Kiselev, A., Stratmann, F., George, I., Baltensperger, U., 2009. Influence of gas-to-particle partitioning on the hygroscopic and droplet activation behaviour of α-pinene secondary organic aerosol. Physical Chemistry Chemical Physics 11, 8091-8097.

Kanakidou, M., Seinfeld, J.H., Pandis, S.N., Barnes, I., Dentener, F.J., Facchini, M.C., Van Dingenen, R., Ervens, B., Nenes, A., Nielsen, C.J., Swietlicki, E., Putaud, J.P., Balkanski, Y., Fuzzi, S., Horth, J., Moortgat, G.K., Winterhalter, R., Myhre, C.E.L., Tsigaridis, K., Vignati, E., Stephanou, E.G., Wilson, J., 2005. Organic aerosol and global climate modelling: a review. Atmospheric Chemistry and Physics 5, 1053-1123.

Kazil, J., Stier, P., Zhang, K., Quaas, J., Kinne, S., O'Donnell, D., Rast, S., Esch, M., Ferrachat, S., Lohmann, U., Feichter, J., 2010. Aerosol nucleation and its role for clouds and Earth's radiative forcing in the aerosol-climate model ECHAM5-HAM. Atmos. Chem. Phys. 10, 10733-10752.

King, S.M., Rosenoern, T., Shilling, J.E., Chen, Q., Martin, S.T., 2007. Cloud condensation nucleus activity of secondary organic aerosol particles mixed with sulfate. Geophysical Research Letters 34.

King, S.M., Rosenoern, T., Shilling, J.E., Chen, Q., Martin, S.T., 2009. Increased cloud activation potential of secondary organic aerosol for atmospheric mass loadings. Atmos. Chem. Phys. 9, 2959-2971.

Kreidenweis, S.M., Koehler, K., DeMott, P.J., Prenni, A.J., Carrico, C., Ervens, B., 2005. Water activity and activation diameters from hygroscopicity data - Part I: Theory and application to inorganic salts. Atmospheric Chemistry and Physics 5, 1357-1370.

Krieger, U.K., Marcolli, C., Reid, J.P., 2012. Exploring the complexity of aerosol particle properties and processes using single particle techniques. Chemical Society Reviews 41, 6631-6662.

Lambe, A.T., Chhabra, P.S., Onasch, T.B., Brune, W.H., Hunter, J.F., Kroll, J.H., Cummings, M.J., Brogan, J.F., Parmar, Y., Worsnop, D.R., Kolb, C.E., Davidovits, P., 2015. Effect of oxidant concentration, exposure time, and seed particles on secondary organic aerosol chemical composition and yield. Atmos. Chem. Phys. 15, 3063-3075.

Lee, A., Goldstein, A.H., Kroll, J.H., Ng, N.L., Varutbangkul, V., Flagan, R.C., Seinfeld, J.H., 2006. Gas-phase products and secondary aerosol yields from the photooxidation of 16 different terpenes. Journal of Geophysical Research: Atmospheres 111.

Liu, P., Song, M., Zhao, T., Gunthe, S.S., Ham, S., He, Y., Qin, Y.M., Gong, Z., Amorim, J.C., Bertram, A.K., Martin, S.T., 2018. Resolving the mechanisms of hygroscopic growth and cloud condensation nuclei activity for organic particulate matter. Nature Communications 9, 4076.

Liu, X., Wang, J., 2010. How important is organic aerosol hygroscopicity to aerosol indirect forcing? Environmental Research Letters 5, 044010.

Marcolli, C., Luo, B., Peter, T., 2004. Mixing of the Organic Aerosol Fractions: Liquids as the Thermodynamically Stable Phases. The Journal of Physical Chemistry A 108, 2216-2224.

Massoli, P., Lambe, A.T., Ahern, A.T., Williams, L.R., Ehn, M., Mikkilä, J., Canagaratna, M.R., Brune, W.H., Onasch, T.B., Jayne, J.T., Petäjä, T., Kulmala, M., Laaksonen, A., Kolb, C.E., Davidovits, P., Worsnop, D.R., 2010. Relationship between aerosol oxidation level and hygroscopic properties of laboratory generated secondary organic aerosol (SOA) particles. Geophysical Research Letters 37.

Meng, L., Coeur, C., Fayad, L., Houzel, N., Genevray, P., Bouzidi, H., Tomas, A., Chen, W., 2020. Secondary organic aerosol formation from the gas-phase reaction of guaiacol (2-methoxyphenol) with NO3 radicals. Atmospheric Environment 240, 117740.

Meyer, N.K., Duplissy, J., Gysel, M., Metzger, A., Dommen, J., Weingartner, E., Alfarra, M.R., Prevot, A.S.H., Fletcher, C., Good, N., McFiggans, G., Jonsson, Å.M., Hallquist, M., Baltensperger, U., Ristovski, Z.D., 2009a. Analysis of the hygroscopic and volatile properties of ammonium sulphate seeded and unseeded SOA particles. Atmos. Chem. Phys. 9, 721-732.

Meyer, N.K., Duplissy, J., Gysel, M., Metzger, A., Dommen, J., Weingartner, E., Alfarra, M.R., Prevot, A.S.H., Fletcher, C., Good, N., McFiggans, G., Jonsson, Å.M., Hallquist, M., Baltensperger, U., Ristovski, Z.D., 2009b. Analysis of the hygroscopic and volatile

properties of ammonium sulphate seeded and unseeded SOA particles. Atmospheric Chemistry and Physics 9, 721-732.

Mikhailov, E., Vlasenko, S., Martin, S.T., Koop, T., Pöschl, U., 2009. Amorphous and crystalline aerosol particles interacting with water vapor: conceptual framework and experimental evidence for restructuring, phase transitions and kinetic limitations. Atmospheric Chemistry and Physics 9, 9491-9522.

Mikhailov, E.F., Pöhlker, M.L., Reinmuth-Selzle, K., Vlasenko, S.S., Krüger, O.O., Fröhlich-Nowoisky, J., Pöhlker, C., Ivanova, O.A., Kiselev, A.A., Kremper, L.A., Pöschl, U., 2021. Water uptake of subpollen aerosol particles: hygroscopic growth, cloud condensation nuclei activation, and liquid–liquid phase separation. Atmos. Chem. Phys. 21, 6999-7022.

Moise, T., Flores, J.M., Rudich, Y., 2015. Optical Properties of Secondary Organic Aerosols and Their Changes by Chemical Processes. Chemical Reviews 115, 4400-4439.

Moore, R.H., Nenes, A., Medina, J., 2010. Scanning Mobility CCN Analysis—A Method for Fast Measurements of Size-Resolved CCN Distributions and Activation Kinetics. Aerosol Science and Technology 44, 861-871.

Ovadnevaite, J., Zuend, A., Laaksonen, A., Sanchez, K.J., Roberts, G., Ceburnis, D., Decesari, S., Rinaldi, M., Hodas, N., Facchini, M.C., Seinfeld, J.H., C, O.D., 2017. Surface tension prevails over solute effect in organic-influenced cloud droplet activation. Nature 546, 637-641.

Pagonis, D., Algrim, L.B., Price, D.J., Day, D.A., Handschy, A.V., Stark, H., Miller, S.L., de Gouw, J.A., Jimenez, J.L., Ziemann, P.J., 2019. Autoxidation of Limonene Emitted in a University Art Museum. Environmental Science & Technology Letters 6, 520-524.

Pajunoja, A., Lambe, A.T., Hakala, J., Rastak, N., Cummings, M.J., Brogan, J.F., Hao, L., Paramonov, M., Hong, J., Prisle, N.L., Malila, J., Romakkaniemi, S., Lehtinen, K.E.J., Laaksonen, A., Kulmala, M., Massoli, P., Onasch, T.B., Donahue, N.M., Riipinen, I., Davidovits, P., Worsnop, D.R., Petäjä, T., Virtanen, A., 2015. Adsorptive uptake of water by semisolid secondary organic aerosols. Geophysical Research Letters 42, 3063-3068.

Pankow, J.F., Asher, W.E., 2008. SIMPOL.1: a simple group contribution method for predicting vapor pressures and enthalpies of vaporization of multifunctional organic compounds. Atmos. Chem. Phys. 8, 2773-2796.

Petters, M.D., Carrico, C.M., Kreidenweis, S.M., Prenni, A.J., DeMott, P.J., Collett Jr., J.L., Moosmüller, H., 2009a. Cloud condensation nucleation activity of biomass burning aerosol. Journal of Geophysical Research: Atmospheres 114.

Petters, M.D., Kreidenweis, S.M., 2007. A single parameter representation of hygroscopic growth and cloud condensation nucleus activity. Atmospheric Chemistry and Physics 7, 1961-1971.

Petters, M.D., Kreidenweis, S.M., 2013. A single parameter representation of hygroscopic growth and cloud condensation nucleus activity – Part 3: Including surfactant partitioning. Atmos. Chem. Phys. 13, 1081-1091.

Petters, M.D., Kreidenweis, S.M., Prenni, A.J., Sullivan, R.C., Carrico, C.M., Koehler, K.A., Ziemann, P.J., 2009b. Role of molecular size in cloud droplet activation. Geophysical Research Letters 36.

Petters, M.D., Wex, H., Carrico, C.M., Hallbauer, E., Massling, A., McMeeking, G.R., Poulain, L., Wu, Z., Kreidenweis, S.M., Stratmann, F., 2009c. Towards closing the gap between hygroscopic growth and activation for secondary organic aerosol – Part 2: Theoretical approaches. Atmospheric Chemistry and Physics 9, 3999-4009.

Pöschl, U., Martin, S.T., Sinha, B., Chen, Q., Gunthe, S.S., Huffman, J.A., Borrmann, S., Farmer, D.K., Garland, R.M., Helas, G., Jimenez, J.L., King, S.M., Manzi, A., Mikhailov, E., Pauliquevis, T., Petters, M.D., Prenni, A.J., Roldin, P., Rose, D., Schneider, J., Su, H., Zorn, S.R., Artaxo, P., Andreae, M.O., 2010. Rainforest Aerosols as Biogenic Nuclei of Clouds and Precipitation in the Amazon. Science 329, 1513-1516.

Poulain, L., Wu, Z., Petters, M.D., Wex, H., Hallbauer, E., Wehner, B., Massling, A., Kreidenweis, S.M., Stratmann, F., 2010. Towards closing the gap between hygroscopic growth and CCN activation for secondary organic aerosols – Part 3: Influence of the chemical composition on the hygroscopic properties and volatile fractions of aerosols. Atmos. Chem. Phys. 10, 3775-3785.

Prenni, A.J., Petters, M.D., Kreidenweis, S.M., DeMott, P.J., Ziemann, P.J., 2007. Cloud droplet activation of secondary organic aerosol. Journal of Geophysical Research: Atmospheres 112.

Prisle, N.L., Lin, J.J., Purdue, S., Lin, H., Meredith, J.C., Nenes, A., 2019. Cloud condensation nuclei activity of six pollenkitts and the influence of their surface activity. Atmos. Chem. Phys. 19, 4741-4761.

Prisle, N.L., Raatikainen, T., Sorjamaa, R., Svenningsson, B., Laaksonen, A., Bilde, M., 2008. Surfactant partitioning in cloud droplet activation: a study of C8, C10, C12 and C14 normal fatty acid sodium salts. Tellus B: Chemical and Physical Meteorology 60, 416-431.

Rastak, N., Pajunoja, A., Acosta Navarro, J.C., Ma, J., Song, M., Partridge, D.G., Kirkevag, A., Leong, Y., Hu, W.W., Taylor, N.F., Lambe, A., Cerully, K., Bougiatioti, A., Liu, P., Krejci, R., Petaja, T., Percival, C., Davidovits, P., Worsnop, D.R., Ekman, A.M.L., Nenes, A., Martin, S., Jimenez, J.L., Collins, D.R., Topping, D.O., Bertram, A.K., Zuend, A., Virtanen, A., Riipinen, I., 2017. Microphysical explanation of the RH-dependent water affinity of biogenic organic aerosol and its importance for climate. Geophysical Research Letters 44, 5167-5177.

Renbaum-Wolff, L., Song, M., Marcolli, C., Zhang, Y., Liu, P.F., Grayson, J.W., Geiger, F.M., Martin, S.T., Bertram, A.K., 2016. Observations and implications of liquid–liquid phase separation at high relative humidities in secondary organic material produced by α-pinene ozonolysis without inorganic salts. Atmos. Chem. Phys. 16, 7969-7979.

Rim, D., Green, M., Wallace, L., Persily, A., Choi, J.-I., 2012. Evolution of Ultrafine Particle Size Distributions Following Indoor Episodic Releases: Relative Importance of Coagulation, Deposition and Ventilation. Aerosol Science and Technology 46, 494-503.

Roberts, G.C., Nenes, A., 2005. A Continuous-Flow Streamwise Thermal-Gradient CCN Chamber for Atmospheric Measurements. Aerosol Science and Technology 39, 206-221.

Rose, D., Gunthe, S.S., Mikhailov, E., Frank, G.P., Dusek, U., Andreae, M.O., Pöschl, U., 2008. Calibration and measurement uncertainties of a continuous-flow cloud condensation nuclei counter (DMT-CCNC): CCN activation of ammonium sulfate and

sodium chloride aerosol particles in theory and experiment. Atmos. Chem. Phys. 8, 1153-1179.

Ruehl, C.R., Chuang, P.Y., Nenes, A., Cappa, C.D., Kolesar, K.R., Goldstein, A.H., 2012. Strong evidence of surface tension reduction in microscopic aqueous droplets. Geophysical Research Letters 39.

Ruehl, C.R., Davies, J.F., Wilson, K.R., 2016. An interfacial mechanism for cloud droplet formation on organic aerosols. Science 351, 1447-1450.

Saathoff, H., Naumann, K.H., Schnaiter, M., Schöck, W., Möhler, O., Schurath, U., Weingartner, E., Gysel, M., Baltensperger, U., 2003. Coating of soot and (NH4)2SO4 particles by ozonolysis products of α-pinene. Journal of Aerosol Science 34, 1297-1321.

Sareen, N., Schwier, A.N., Lathem, T.L., Nenes, A., McNeill, V.F., 2013. Surfactants from the gas phase may promote cloud droplet formation. Proceedings of the National Academy of Sciences 110, 2723-2728.

Schervish, M., Donahue, N.M., 2020. Peroxy radical chemistry and the volatility basis set. Atmos. Chem. Phys. 20, 1183-1199.

Schervish, M., Donahue, N.M., 2021. Peroxy radical kinetics and new particle formation. Environmental Science: Atmospheres 1, 79-92.

Scott, C.E., Rap, A., Spracklen, D.V., Forster, P.M., Carslaw, K.S., Mann, G.W., Pringle, K.J., Kivekäs, N., Kulmala, M., Lihavainen, H., Tunved, P., 2014. The direct and indirect radiative effects of biogenic secondary organic aerosol. Atmos. Chem. Phys. 14, 447-470.

Setyan, A., Song, C., Merkel, M., Knighton, W.B., Onasch, T.B., Canagaratna, M.R., Worsnop, D.R., Wiedensohler, A., Shilling, J.E., Zhang, Q., 2014. Chemistry of new particle growth in mixed urban and biogenic emissions – insights from CARES. Atmos. Chem. Phys. 14, 6477-6494.

Shilling, J.E., Chen, Q., King, S.M., Rosenoern, T., Kroll, J.H., Worsnop, D.R., DeCarlo, P.F., Aiken, A.C., Sueper, D., Jimenez, J.L., Martin, S.T., 2009. Loading-dependent elemental composition of α-pinene SOA particles. Atmos. Chem. Phys. 9, 771-782.

Smith, M.L., Bertram, A.K., Martin, S.T., 2012. Deliquescence, efflorescence, and phase miscibility of mixed particles of ammonium sulfate and isoprene-derived secondary organic material. Atmos. Chem. Phys. 12, 9613-9628.

Smith, M.L., Kuwata, M., Martin, S.T., 2011. Secondary Organic Material Produced by the Dark Ozonolysis of α-Pinene Minimally Affects the Deliquescence and Efflorescence of Ammonium Sulfate. Aerosol Science and Technology 45, 244-261.

Smith, M.L., You, Y., Kuwata, M., Bertram, A.K., Martin, S.T., 2013. Phase Transitions and Phase Miscibility of Mixed Particles of Ammonium Sulfate, Toluene-Derived Secondary Organic Material, and Water. The Journal of Physical Chemistry A 117, 8895-8906.

Song, M., Liu, P., Martin, S.T., Bertram, A.K., 2017. Liquid–liquid phase separation in particles containing secondary organic material free of inorganic salts. Atmos. Chem. Phys. 17, 11261-11271.

Spracklen, D.V., Jimenez, J.L., Carslaw, K.S., Worsnop, D.R., Evans, M.J., Mann, G.W., Zhang, Q., Canagaratna, M.R., Allan, J., Coe, H., McFiggans, G., Rap, A.,

Forster, P., 2011. Aerosol mass spectrometer constraint on the global secondary organic aerosol budget. Atmos. Chem. Phys. 11, 12109-12136.

Su, H., Rose, D., Cheng, Y.F., Gunthe, S.S., Massling, A., Stock, M., Wiedensohler, A., Andreae, M.O., Pöschl, U., 2010. Hygroscopicity distribution concept for measurement data analysis and modeling of aerosol particle mixing state with regard to hygroscopic growth and CCN activation. Atmos. Chem. Phys. 10, 7489-7503.

Swietlicki, E., Hansson, H.C., Hämeri, K., Svenningsson, B., Massling, A., McFiggans, G., McMurry, P.H., Petäjä, T., Tunved, P., Gysel, M., Topping, D., Weingartner, E., Baltensperger, U., Rissler, J., Wiedensohler, A., Kulmala, M., 2017. Hygroscopic properties of submicrometer atmospheric aerosol particles measured with H-TDMA instruments in various environments—a review. Tellus B: Chemical and Physical Meteorology 60, 432-469.

Tang, X., Cocker Iii, D.R., Asa-Awuku, A., 2012. Are sesquiterpenes a good source of secondary organic cloud condensation nuclei (CCN)? Revisiting β-caryophyllene CCN. Atmos. Chem. Phys. 12, 8377-8388.

Topping, D.O., Barley, M.H., McFiggans, G., 2011. The sensitivity of Secondary Organic Aerosol component partitioning to the predictions of component properties – Part 2: Determination of particle hygroscopicity and its dependence on "apparent" volatility. Atmos. Chem. Phys. 11, 7767-7779.

Topping, D.O., McFiggans, G., 2012. Tight coupling of particle size, number and composition in atmospheric cloud droplet activation. Atmos. Chem. Phys. 12, 3253-3260.

Tritscher, T., Dommen, J., DeCarlo, P.F., Gysel, M., Barmet, P.B., Praplan, A.P., Weingartner, E., Prévôt, A.S.H., Riipinen, I., Donahue, N.M., Baltensperger, U., 2011. Volatility and hygroscopicity of aging secondary organic aerosol in a smog chamber. Atmos. Chem. Phys. 11, 11477-11496.

Tsigaridis, K., Daskalakis, N., Kanakidou, M., Adams, P.J., Artaxo, P., Bahadur, R., Balkanski, Y., Bauer, S.E., Bellouin, N., Benedetti, A., Bergman, T., Berntsen, T.K., Beukes, J.P., Bian, H., Carslaw, K.S., Chin, M., Curci, G., Diehl, T., Easter, R.C., Ghan, S.J., Gong, S.L., Hodzic, A., Hoyle, C.R., Iversen, T., Jathar, S., Jimenez, J.L., Kaiser, J.W., Kirkevåg, A., Koch, D., Kokkola, H., Lee, Y.H., Lin, G., Liu, X., Luo, G., Ma, X., Mann, G.W., Mihalopoulos, N., Morcrette, J.J., Müller, J.F., Myhre, G., Myriokefalitakis, S., Ng, N.L., O'Donnell, D., Penner, J.E., Pozzoli, L., Pringle, K.J., Russell, L.M., Schulz, M., Sciare, J., Seland, Ø., Shindell, D.T., Sillman, S., Skeie, R.B., Spracklen, D., Stavrakou, T., Steenrod, S.D., Takemura, T., Tiitta, P., Tilmes, S., Tost, H., van Noije, T., van Zyl, P.G., von Salzen, K., Yu, F., Wang, Z., Wang, Z., Zaveri, R.A., Zhang, H., Zhang, K., Zhang, Q., Zhang, X., 2014. The AeroCom evaluation and intercomparison of organic aerosol in global models. Atmos. Chem. Phys. 14, 10845-10895.

Väisänen, O., Ruuskanen, A., Ylisirniö, A., Miettinen, P., Portin, H., Hao, L., Leskinen, A., Komppula, M., Romakkaniemi, S., Lehtinen, K.E.J., Virtanen, A., 2016. In-cloud measurements highlight the role of aerosol hygroscopicity in cloud droplet formation. Atmospheric Chemistry and Physics 16, 10385-10398.

VanReken, T.M., Ng, N.L., Flagan, R.C., Seinfeld, J.H., 2005. Cloud condensation nucleus activation properties of biogenic secondary organic aerosol. Journal of Geophysical Research: Atmospheres 110.

Varutbangkul, V., Brechtel, F.J., Bahreini, R., Ng, N.L., Keywood, M.D., Kroll, J.H., Flagan, R.C., Seinfeld, J.H., Lee, A., Goldstein, A.H., 2006. Hygroscopicity of secondary organic aerosols formed by oxidation of cycloalkenes, monoterpenes, sesquiterpenes, and related compounds. Atmos. Chem. Phys. 6, 2367-2388.

Virkkula, A., Van Dingenen, R., Raes, F., Hjorth, J., 1999. Hygroscopic properties of aerosol formed by oxidation of limonene, α-pinene, and β-pinene. Journal of Geophysical Research: Atmospheres 104, 3569-3579.

Wang, Y., Voliotis, A., Hu, D., Shao, Y., Du, M., Chen, Y., Alfarra, M.R., McFiggans, G., 2021. On the evolution of sub- and super-saturated water uptake of secondary organic aerosol in chamber experiments from mixed precursors. Atmos. Chem. Phys. Discuss. 2021, 1-30.

Wex, H., Petters, M.D., Carrico, C.M., Hallbauer, E., Massling, A., McMeeking, G.R., Poulain, L., Wu, Z., Kreidenweis, S.M., Stratmann, F., 2009. Towards closing the gap between hygroscopic growth and activation for secondary organic aerosol: Part 1 – Evidence from measurements. Atmos. Chem. Phys. 9, 3987-3997.

Wex, H., Stratmann, F., Topping, D., McFiggans, G., 2008. The Kelvin versus the Raoult Term in the Köhler Equation. Journal of the Atmospheric Sciences 65, 4004-4016.

Winkler, P.M., Ortega, J., Karl, T., Cappellin, L., Friedli, H.R., Barsanti, K., McMurry, P.H., Smith, J.N., 2012. Identification of the biogenic compounds responsible for size-dependent nanoparticle growth. Geophysical Research Letters 39.

Wittbom, C., Eriksson, A.C., Rissler, J., Roldin, P., Nordin, E.Z., Sjogren, S., Nilsson, P.T., Swietlicki, E., Pagels, J., Svenningsson, B., 2018. Effect of solubility limitation on hygroscopic growth and cloud drop activation of SOA particles produced from traffic exhausts. Journal of Atmospheric Chemistry 75, 359-383.

Wu, J., Faccinetto, A., Grimonprez, S., Batut, S., Yon, J., Desgroux, P., Petitprez, D., 2020. Influence of the dry aerosol particle size distribution and morphology on the cloud condensation nuclei activation. An experimental and theoretical investigation. Atmos. Chem. Phys. 20, 4209-4225.

Wu, Z.J., Poulain, L., Henning, S., Dieckmann, K., Birmili, W., Merkel, M., van Pinxteren, D., Spindler, G., Müller, K., Stratmann, F., Herrmann, H., Wiedensohler, A., 2013. Relating particle hygroscopicity and CCN activity to chemical composition during the HCCT-2010 field campaign. Atmos. Chem. Phys. 13, 7983-7996.

Xavier, C., Rusanen, A., Zhou, P., Dean, C., Pichelstorfer, L., Roldin, P., Boy, M., 2019. Aerosol mass yields of selected biogenic volatile organic compounds – a theoretical study with nearly explicit gas-phase chemistry. Atmos. Chem. Phys. 19, 13741-13758.

Xu, L., Pye, H.O.T., He, J., Chen, Y., Murphy, B.N., Ng, N.L., 2018. Experimental and model estimates of the contributions from biogenic monoterpenes and sesquiterpenes to secondary organic aerosol in the southeastern United States. Atmos. Chem. Phys. 18, 12613-12637.

Xu, L., Tsona, N.T., You, B., Zhang, Y., Wang, S., Yang, Z., Xue, L., Du, L., 2020. NOx enhances secondary organic aerosol formation from nighttime γ-terpinene ozonolysis. Atmospheric Environment 225, 117375.

Yáñez-Serrano, A.M., Nölscher, A.C., Bourtsoukidis, E., Gomes Alves, E., Ganzeveld, L., Bonn, B., Wolff, S., Sa, M., Yamasoe, M., Williams, J., Andreae, M.O., Kesselmeier,

J., 2018. Monoterpene chemical speciation in a tropical rainforest:variation with season, height, and time of dayat the Amazon Tall Tower Observatory (ATTO). Atmos. Chem. Phys. 18, 3403-3418.

Yu, M., Koivisto, A.J., Hämeri, K., Seipenbusch, M., 2013. Size Dependence of the Ratio of Aerosol Coagulation to Deposition Rates for Indoor Aerosols. Aerosol Science and Technology 47, 427-434.

Yuan, C., Ma, Y., Diao, Y., Yao, L., Zhou, Y., Wang, X., Zheng, J., 2017. CCN activity of secondary aerosols from terpene ozonolysis under atmospheric relevant conditions. Journal of Geophysical Research: Atmospheres 122, 4654-4669.

Zhang, H., Yee, L.D., Lee, B.H., Curtis, M.P., Worton, D.R., Isaacman-VanWertz, G., Offenberg, J.H., Lewandowski, M., Kleindienst, T.E., Beaver, M.R., Holder, A.L., Lonneman, W.A., Docherty, K.S., Jaoui, M., Pye, H.O.T., Hu, W., Day, D.A., Campuzano-Jost, P., Jimenez, J.L., Guo, H., Weber, R.J., de Gouw, J., Koss, A.R., Edgerton, E.S., Brune, W., Mohr, C., Lopez-Hilfiker, F.D., Lutz, A., Kreisberg, N.M., Spielman, S.R., Hering, S.V., Wilson, K.R., Thornton, J.A., Goldstein, A.H., 2018. Monoterpenes are the largest source of summertime organic aerosol in the southeastern United States. Proceedings of the National Academy of Sciences 115, 2038-2043.

Zhang, Q., Jimenez, J.L., Canagaratna, M.R., Allan, J.D., Coe, H., Ulbrich, I., Alfarra, M.R., Takami, A., Middlebrook, A.M., Sun, Y.L., Dzepina, K., Dunlea, E., Docherty, K., DeCarlo, P.F., Salcedo, D., Onasch, T., Jayne, J.T., Miyoshi, T., Shimono, A., Hatakeyama, S., Takegawa, N., Kondo, Y., Schneider, J., Drewnick, F., Borrmann, S., Weimer, S., Demerjian, K., Williams, P., Bower, K., Bahreini, R., Cottrell, L., Griffin, R.J., Rautiainen, J., Sun, J.Y., Zhang, Y.M., Worsnop, D.R., 2007. Ubiquity and dominance of oxygenated species in organic aerosols in anthropogenically-influenced Northern Hemisphere midlatitudes. Geophysical Research Letters 34, L13801.

Zhao, D., Pullinen, I., Fuchs, H., Schrade, S., Wu, R., Acir, I.H., Tillmann, R., Rohrer, F., Wildt, J., Guo, Y., Kiendler-Scharr, A., Wahner, A., Kang, S., Vereecken, L., Mentel, T.F., 2021. Highly oxygenated organic molecule (HOM) formation in the isoprene oxidation by NO3 radical. Atmos. Chem. Phys. 21, 9681-9704.

Zhao, D.F., Buchholz, A., Kortner, B., Schlag, P., Rubach, F., Fuchs, H., Kiendler-Scharr, A., Tillmann, R., Wahner, A., Watne, Å.K., Hallquist, M., Flores, J.M., Rudich, Y., Kristensen, K., Hansen, A.M.K., Glasius, M., Kourtchev, I., Kalberer, M., Mentel, T.F., 2016. Cloud condensation nuclei activity, droplet growth kinetics, and hygroscopicity of biogenic and anthropogenic secondary organic aerosol (SOA). Atmos. Chem. Phys. 16, 1105-1121.

Zhao, D.F., Buchholz, A., Kortner, B., Schlag, P., Rubach, F., Kiendler-Scharr, A., Tillmann, R., Wahner, A., Flores, J.M., Rudich, Y., Watne, Å.K., Hallquist, M., Wildt, J., Mentel, T.F., 2015. Size-dependent hygroscopicity parameter (κ) and chemical composition of secondary organic cloud condensation nuclei. Geophysical Research Letters 42, 10,920-910,928.

Zieger, P., Fierz-Schmidhauser, R., Gysel, M., Ström, J., Henne, S., Yttri, K.E., Baltensperger, U., Weingartner, E., 2010. Effects of relative humidity on aerosol light scattering in the Arctic. Atmospheric Chemistry and Physics 10, 3875-3890.

Zuend, A., Marcolli, C., Luo, B.P., Peter, T., 2008. A thermodynamic model of mixed organic-inorganic aerosols to predict activity coefficients. Atmospheric Chemistry and Physics 8, 4559-4593.

Zuend, A., Seinfeld, J.H., 2012. Modeling the gas-particle partitioning of secondary organic aerosol: the importance of liquid-liquid phase separation. Atmospheric Chemistry and Physics 12, 3857-3882.